J. Fluid Mech. (2006), *vol.* 567, *pp.* 195–233. © 2006 Cambridge University Press
doi:10.1017/S002211200600214X Printed in the United Kingdom

Algebraic and exponential instabilities in a sheared micropolar granular fluid

By BISHAKHDATTA GAYEN AND MEHEBOOB ALAM†

Engineering Mechanics Unit, Jawaharlal Nehru Center for Advanced Scientific Research, Jakkur PO, Bangalore 560064, India

(Received 13 November 2005 and in revised form 4 May 2006)

Based on a micropolar continuum of rough granular particles that takes into account the balance equations for the spin (/rotational) velocity and the spin granular temperature, the linear stability characteristics of an unbounded shear flow ($\boldsymbol{u} \equiv (u_x, u_y, u_z) = (\dot{\gamma} y, 0, 0)$, where x, y and z are the streamwise, transverse and spanwise directions, respectively, and $\dot{\gamma}$ is the shear rate) are analysed. For pure spanwise perturbations ($k_z \neq 0$, with $k_x = 0 = k_y$, where k_i is the wavenumber in the ith direction), we show that the streamwise translational velocity and the transverse spin velocity modes are subject to linear growths, owing to an inviscid 'algebraic' instability (that grows linearly with time). This algebraic instability is shown to be tied to a hidden mechanism of momentum transfer from the translational to the rotational modes, via pure spanwise perturbations to the transverse velocity – in short, we have uncovered an 'instability-induced rotational-driving' mechanism. Pure spanwise ($k_z \neq 0$, with $k_x = 0 = k_y$) and pure transverse ($k_y \neq 0$, with $k_x = 0 = k_z$) perturbations give rise to 'exponential' instabilities (that grow exponentially with time) which are related to similar stationary instabilities in the shear flow of smooth, inelastic particles. Both these instabilities also survive in the limiting case of perfectly elastic but rough particles. The scalings of hydrodynamic modes with wavenumbers have been obtained via the respective long-wave expansion. Perturbations with modulations in all three directions are shown to be stable in the asymptotic time limit, but there could be short-time 'exponential' growth of these general perturbations in the long-wave limit for both travelling and stationary waves. The growth rate of all instabilities is maximum at intermediate values of the tangential restitution coefficient (β), and decreases in both the perfectly smooth ($\beta \to -1$) and rough ($\beta \to 1$) limits; the associated instability length scale is minimum at intermediate β, and increases in both the perfectly smooth and rough limits. In the perfectly smooth limit, there is a window of particle volume fraction (ϕ), $\phi_c^s < \phi < \phi_c^t$, over which the flow remains stable to all perturbations. With the inclusion of spin fields, the size of this window decreases and at moderate dissipations with $\beta > 0.5$ the flow becomes unstable at all ϕ.

1. Introduction

During the last two decades, much work has been devoted to understanding the rheology (see, for reviews, Savage 1984; Hutter & Rajagopal 1994) and, more recently, the dynamics of granular materials (see, for reviews, Jaeger, Nagel & Behringer 1996; Herrmann, Hovi & Luding 1998; Kadanoff 1999; Goldhirsch 2003). In the rapid

† Author to whom correspondence should be addressed: meheboob@jncasr.ac.in.

https://doi.org/10.1017/S002211200600214X Published online by Cambridge University Press

flow regime in which the particles move around randomly, interacting mainly via instantaneous *dissipative* collisions with negligible interstitial fluid effects, the granular material has been modelled as a system of smooth inelastic hard spheres. The standard statistical mechanical tools of the kinetic theory of dense gases have been modified to develop appropriate rheological models for a continuum description of such fluidized granular materials (Lun *et al.* 1984; Jenkins & Richman 1985; Goldshtein & Shapiro 1995; Sela & Goldhirsch 1998; Montanero *et al.* 1999). If the particles are smooth, their collisions can be characterized by a single parameter, the normal restitution coefficient (e), with the limiting case of $e = 1$ being tied with elastic collisions and no energy loss. It is now well-known that this 'added' inelasticity is a source of many interesting and unresolved phenomena in granular flows.

The stability analyses of granular shear flows have attracted much attention recently (Savage 1992; Babic 1993; Schmid & Kytömaa 1994; Wang, Jackson & Sundaresan 1996; Alam & Nott 1997, 1998; Tan & Goldhirsch 1997; Alam 2005, 2006); the Navier–Stokes-level hydrodynamic equations are routinely used for such analyses. The major motivation of these works has been the desire to understand certain dynamical features of shear flows (clustering or density inhomogeneities, plug formation, etc.; Hopkins, Louge & Jenkins 1993; Goldhirsch & Zanetti 1993; Tan & Goldhirsch 1997; Luding & Herrmann 1999; Conway & Glasser 2004; Alam 2005) as well as to uncover the scalings of the underlying hydrodynamics modes (Mello, Diamond & Levine 1991; McNamara 1993). Explaining the dynamics of granular fluids using continuum equations is a stringent test of the adopted constitutive models. Note that all these stability analyses were carried out using constitutive models for smooth inelastic particles.

Real particles are always characterized by some degrees of roughness, giving rise to surface friction. Consequently, the rotational motion becomes important to deal with rough, frictional particles. Even in the limit of nearly inelastic particles ($e \approx 1$), the added complexity of the rotational motion gives rise to additional hydrodynamic fields: the spin/rotational velocities and the rotational granular temperature (Condiff & Dahler 1964; Theodosopulu & Dahler 1974; Dahler & Theodosopulu 1975; Jenkins & Richman 1985; Lun & Savage 1987; Lun 1991; Luding *et al.* 1998; Mitarai, Hayakawa & Nakanishi 2002; Hayakawa 2003; Goldhirsh, Noskowicz & Bar-Lev 2005). It turns out that the translational and rotational temperatures of a granular fluid are not equally partitioned (Lun & Savage 1987; Lun 1991; Huthmann & Zippelius 1997; McNamara & Luding 1998), except in the perfect rough limit. More importantly, at finite densities, there is an additional contribution to the stress tensor that renders it asymmetric – a signature of the micropolar theory (Condiff & Dahler 1964; Kanatani 1979; Mitarai *et al.* 2002). Another new ingredient associated with rotational motion is the transport via the couple stress (i.e. the flux of angular momentum) which becomes important in the presence of boundaries. The implications of the additional hydrodynamic fields, the energy non-equipartition, the asymmetric stress tensor and the couple stress on the dynamical behaviour of a granular fluid are not known *a priori*, and have not been investigated before for a driven system like shear flow.

The molecular dynamics (MD) simulation work of Moon, Swift & Swinney (2004) has elucidated the role of friction on pattern formation in oscillated granular layers. They found that while the square, stripe and hexagonal patterns are stable for frictional particles (that match with experimental results), only the stripe-pattern is stable for frictionless particles. Certain experimental phenomena (e.g. the parametric sloshing of particles, the shock-wave formation, etc.) also occur in MD simulations

https://doi.org/10.1017/S002211200600214X Published online by Cambridge University Press

with and without friction, but there are important differences in the details of these phenomena. There has been some work on the 'rotational-driving' of a granular fluid (Cafiero, Luding & Herrmann 2002; Luding, Cafiero & Herrmann 2003). These authors showed that a granular fluid can be made spatially homogeneous even at very high dissipation levels by transferring energy from the rotational degrees of freedom to their translational counterpart, even though its (translational) velocity distribution function shows large deviations from a Maxwellian. They also explained some recent experimental results (see, for details, Luding *et al.* 2003) by driving on both the translational and the rotational degrees of freedom. The consensus that emerges from the above discussion is that the rotational motion should not be neglected for a realistic modelling of the dynamics and pattern formation in granular media even in the dilute limit.

In the present paper, we investigate the effects of rotational motion on the stability characteristics of the unbounded shear flow of rough and inelastic particles. A micropolar continuum is used to treat the rotational degrees of freedom: the collision model of rough particles and the balance equations are briefly described in §§ 2.1 and 2.2, respectively; the kinetic-theory-based constitutive model of Lun (1991) is used for the rheology of granular materials as in § 2.3. The non-dimensional balance equations are written down in § 3.1 and the base state of the unbounded uniform shear flow is analysed in § 3.2. The base state of the unbounded shear flow is characterized by a linear streamwise velocity profile, ($\boldsymbol{u} \equiv (u_x, u_y, u_z) = (\dot{\gamma} y, 0, 0)$, where x, y and z are the streamwise, transverse and spanwise directions, respectively, and $\dot{\gamma}$ is the shear rate), with constant values of solid fraction, spanwise spin velocity, and translational and spin granular temperatures. The linear stability problem of this flow is formulated in § 4, via the Kelvin-mode decomposition. The stability results for streamwise-independent perturbations (as well as the scalings of hydrodynamic modes with wavenumbers) are presented and discussed in § 5. We have uncovered an inviscid algebraic instability (see § 5.1 for details) for pure spanwise perturbations that is directly connected to a hidden mechanism of momentum transfer from the translational degrees of freedom to their rotational counterparts. Both the long-time and short-time behaviour of streamwise-dependent perturbations ($k_x \neq 0$) are analysed in § 6. The possible effect of Coulomb friction on the observed instabilities is discussed briefly in § 7.1, and the limitations of Lun's constitutive model is discussed in § 7.2. We summarize our results with conclusions in § 8.

2. Micropolar theory for rough inelastic particles

2.1. *Background: collision model*

We consider a monodisperse system of rough inelastic spheres of size σ, mass m, material density ρ_p and the moment of inertia $\mathscr{I}$, interacting via the hard-core potential. The moment of inertia can be expressed in terms of a non-dimensional shape factor:

$$K = \frac{4\mathscr{I}}{m\sigma^2}, \tag{2.1}$$

with $K = 2/5$ for solid spheres and $2/3$ for a thin-shell sphere. The pre-collisional translational and angular velocities of particle i are denoted by $\boldsymbol{c}_i$ and $\boldsymbol{\omega}_i$, respectively, and their post-collisional counterparts by $\boldsymbol{c}_i'$ and $\boldsymbol{\omega}_i'$, respectively. The precollisional relative velocity at contact, $\boldsymbol{g}_{ij}$, between particles i and j is given by

$$\boldsymbol{g}_{ij} = \boldsymbol{c}_{ij} - \boldsymbol{k} \times (\boldsymbol{\omega}_i + \boldsymbol{\omega}_j), \tag{2.2}$$

https://doi.org/10.1017/S002211200600214X Published online by Cambridge University Press

where $\boldsymbol{c}_{ij} = \boldsymbol{c}_i - \boldsymbol{c}_j$ is the translational velocity of the ith particle relative to that of the jth particle, and $\boldsymbol{k}_{ij} = \boldsymbol{x}_{pj} - \boldsymbol{x}_{pi} = \boldsymbol{k}$ the contact vector directed from the centre of the ith particle to that of the jth particle.

For the simplest model of rough inelastic spheres (Lun & Savage 1987), the pre- and post-collisional velocities of the colliding particles are related via the following expressions:

$$\boldsymbol{k}\cdot\boldsymbol{g}'_{ij} = -e(\boldsymbol{k}\cdot\boldsymbol{g}_{ij}), \quad \boldsymbol{k}\times\boldsymbol{g}'_{ij} = -\beta(\boldsymbol{k}\times\boldsymbol{g}_{ij}), \tag{2.3}$$

where e is the normal coefficient of restitution, and β the tangential coefficient of restitution. The former is an indicator of the inelasticity of a particle and the latter an indicator of its surface roughness; in general, $0 \leqslant e \leqslant 1$ and $-1 \leqslant \beta \leqslant 1$. For collisions between perfectly smooth particles, $\beta = -1$, with the increasing value of β being an indicator of the increasing degrees of particle surface friction. The value of $\beta = 0$ represents the case for which the particle surface friction and inelasticity are sufficient to eliminate the post-collisional tangential relative velocities. For $0 < \beta \leqslant 1$, the spin-reversal occurs after collision (Maw, Barber & Fawcett 1981), and the case of $\beta = 1$ corresponds to collisions between perfectly rough particles. For a discussion on collision models with oblique impact and Coulomb friction, and the range of validity of the present constant-β approximation, see Appendix A.

2.2. *Hydrodynamic fields and balance equations*

The hydrodynamic field variables are defined via the standard coarse-graining of the particle-level variables (the particle mass m, its linear momentum $m\boldsymbol{c}$, angular momentum $\mathscr{I}\boldsymbol{\omega}$, translational kinetic energy $mc^2/2$ and rotational kinetic energy $\mathscr{I}\omega^2/2$) using the single-particle velocity distribution function $f(\boldsymbol{x}_p, \boldsymbol{c}, \boldsymbol{\omega}; t)$, where $\boldsymbol{x}_p$ refers to particle's position vector (Dahler & Theodosopulu 1975; Lun 1991).

The coarse-grained mass-density, $\varrho(\boldsymbol{x}, t) = mn = \rho_p\phi$, the translational velocity, $\boldsymbol{u}(\boldsymbol{x}, t)$, and the spin velocity, $\boldsymbol{\Omega}(\boldsymbol{x}, t)$, are defined as

$$\varrho(\boldsymbol{x}, t) = mn = m\int f(\boldsymbol{x}_p, \boldsymbol{c}, \boldsymbol{\omega}; t)\,\mathrm{d}\boldsymbol{c}\,\mathrm{d}\boldsymbol{\omega}, \tag{2.4}$$

$$\boldsymbol{u}(\boldsymbol{x}, t) = \langle\boldsymbol{c}\rangle = \frac{1}{n}\int \boldsymbol{c} f(\boldsymbol{x}_p, \boldsymbol{c}, \boldsymbol{\omega}; t)\,\mathrm{d}\boldsymbol{c}\,\mathrm{d}\boldsymbol{\omega}, \tag{2.5}$$

$$\boldsymbol{\Omega}(\boldsymbol{x}, t) = \langle\boldsymbol{\omega}\rangle = \frac{1}{n}\int \boldsymbol{\omega} f(\boldsymbol{x}_p, \boldsymbol{c}, \boldsymbol{\omega}; t)\,\mathrm{d}\boldsymbol{c}\,\mathrm{d}\boldsymbol{\omega}, \tag{2.6}$$

where $n = n(\boldsymbol{x}, t)$ is the (coarse-grained) particle number density and ϕ the volume fraction of particles ('solid fraction'). The coarse-grained 'translational' fluctuation kinetic energy (i.e. the standard granular temperature), $T(\boldsymbol{x}, t)$, and the rotational fluctuation kinetic energy, $\theta(\boldsymbol{x}, t)$, are defined as

$$T(\boldsymbol{x}, t) = \tfrac{1}{3}\langle\boldsymbol{C}\cdot\boldsymbol{C}\rangle = \tfrac{1}{3}\langle C^2\rangle, \tag{2.7}$$

$$\theta(\boldsymbol{x}, t) = \frac{\mathscr{I}}{3m}\langle\boldsymbol{W}\cdot\boldsymbol{W}\rangle = \frac{\mathscr{I}}{3m}\langle W^2\rangle. \tag{2.8}$$

These two higher-order hydrodynamic fields are required as the transport coefficients are functions of T and θ. Here, $\boldsymbol{C} = \boldsymbol{c} - \boldsymbol{u}$ is the peculiar velocity (that measures the deviation of the instantaneous particle velocity from the local mean velocity). Similar to the peculiar velocity, $\boldsymbol{W} = \boldsymbol{\omega} - \boldsymbol{\Omega}$ measures the deviation of the instantaneous particle spin from the local mean spin velocity.

https://doi.org/10.1017/S002211200600214X Published online by Cambridge University Press

The balance equations for mass, linear momentum, angular momentum, translational granular temperature and rotational granular temperature are:

$$\frac{\partial \varrho}{\partial t} + \nabla \cdot (\varrho \boldsymbol{u}) = 0, \tag{2.9}$$

$$\varrho \left(\frac{\partial}{\partial t} + \boldsymbol{u} \cdot \nabla \right) \boldsymbol{u} = -\nabla \cdot \boldsymbol{P} + \varrho \boldsymbol{b}, \tag{2.10}$$

$$n\mathscr{I} \left(\frac{\partial}{\partial t} + \boldsymbol{u} \cdot \nabla \right) \boldsymbol{\Omega} = -\nabla \cdot \boldsymbol{G} + \boldsymbol{\Psi} + \varrho \boldsymbol{b}_c, \tag{2.11}$$

$$\tfrac{3}{2}\varrho \left(\frac{\partial}{\partial t} + \boldsymbol{u} \cdot \nabla \right) T = -\nabla \cdot \boldsymbol{q} - \boldsymbol{P} : \nabla \boldsymbol{u} - \mathscr{D}, \tag{2.12}$$

$$\tfrac{3}{2}\varrho \left(\frac{\partial}{\partial t} + \boldsymbol{u} \cdot \nabla \right) \theta = -\nabla \cdot \boldsymbol{q}_r - \boldsymbol{G} : \nabla \boldsymbol{\Omega} - \mathscr{D}_r - \boldsymbol{\Omega} \cdot \boldsymbol{\Psi}, \tag{2.13}$$

respectively. Here, $\boldsymbol{P}$ is the stress tensor (linear momentum flux), $\boldsymbol{G}$ the angular momentum flux (couple stress), $\boldsymbol{b}$ the external body force per unit mass, $\boldsymbol{b}_c$ the external body couple per unit mass, $\boldsymbol{\Psi}$ the source of angular momentum, $\boldsymbol{q}$ the translational granular heat flux, $\boldsymbol{q}_r$ the rotational granular heat flux, $\mathscr{D}$ the rate of dissipation of translational granular energy per unit volume, and $\mathscr{D}_r$ the rate of dissipation of rotational granular energy per unit volume. The term $\boldsymbol{P} : \nabla \boldsymbol{u}$ in (2.12) represents the rate of production of translational energy due to shear work, and $\boldsymbol{G} : \nabla \boldsymbol{\Omega}$ in (2.13) represents the rate of production of rotational energy.

For inelastic and rough particles, a two-temperature theory should be used since the translational and rotational temperatures are not equally partitioned (except in the perfectly rough limit). The issue of using separate balance equations for T and θ even for a system of elastic rough spheres has been discussed by many (see, for example, McCoy, Sandler & Dahler 1966). It may be noted that the above set of balance equations has also been derived by Babić (1997) for both quasi-static and rapid granular flows using a general weighted space–time averaging technique. Therefore, these balance equations are of a general nature, and can be used for fluids for which the micro-rotation fields play an important role. Of course, the difference appears only in the choice of the constitutive model which depends on the type of the flow that one is interested in.

2.3. *Constitutive model*

We have chosen the constitutive model of Lun (1991) who derived analytical expressions for all flux terms up to the Navier–Stokes-order for rough inelastic particles, using the generalized moment method. For a system of perfectly elastic particles ($e = 1$), this constitutive model boils down to that of Theodosopulu & Dahler (1974) except for the bulk viscosity and the collisional flux of translational energy. On the other hand, in the limit of perfectly smooth ($\beta = -1$), inelastic particles, the model of Lun *et al.* (1984) is recovered. Note that the transport coefficients of the Lun-model (pressure, viscosity and stress-ratio) have been tested via MD simulations of shear flow (Lun & Bent 1994) with a fair agreement between simulation and theory for three different values of $\beta = -1, -0.5, 0$ over a range of volume fractions. The limitations of this constitutive model and the robustness of our stability results for the whole range of $\beta \in (-1, 1)$ are discussed in § 7.2.

The stress tensor can be decomposed as:

$$\boldsymbol{P} = [p - \xi(\nabla \cdot \boldsymbol{u})]\boldsymbol{1} - 2\mu \boldsymbol{S} - \mu_r \boldsymbol{1} \times (2\boldsymbol{\Omega} - \nabla \times \boldsymbol{u}), \tag{2.14}$$

https://doi.org/10.1017/S002211200600214X Published online by Cambridge University Press

with the deviatoric part of the deformation tensor being given by

$$\boldsymbol{S} = \tfrac{1}{2}(\nabla \boldsymbol{u} + \nabla \boldsymbol{u}^T) - \tfrac{1}{3}(\nabla \cdot \boldsymbol{u})\boldsymbol{1}, \tag{2.15}$$

and $\boldsymbol{1}$ is the identity tensor. Here, p is the pressure, and μ, ξ and μ_r are the shear-, bulk- and 'vortex' spin-viscosities, respectively, which are functions of the particle size, number density, solids fraction, granular temperature, etc. Note that there is an additional contribution to the stress tensor that arises from the difference between the rotation due to the translational velocity (i.e. vorticity) and the spin velocity, $\boldsymbol{\Omega}$. This term makes the stress tensor asymmetric, i.e. $P_{ij} \neq P_{ji}$, which is a signature of the micropolar fluid. Note that this term is proportional to the 'vortex' spin viscosity μ_r (hereinafter μ_r will be referred to as the vortex viscosity; Condiff & Dahler 1964) which is a measure of the resistance of the fluid to the rotational motion, and it represents a coupling between the rotation due to the translational velocity and the micro-rotation field itself.

The constitutive expressions for the pressure, the shear viscosity, the bulk viscosity and the vortex viscosity are given by:

$$\left.\begin{aligned} p &= \rho_p T f_1(\phi, e), & \mu &= \rho_p \sigma T^{1/2} f_2(\phi, \theta/T; e, \beta, K), \\ \xi &= \rho_p \sigma T^{1/2} f_3(\phi; e), & \mu_r &= \rho_p \sigma T^{1/2} f_{2r}(\phi; \beta, K). \end{aligned}\right\} \tag{2.16}$$

where $f_i(\cdot)$ are non-dimensional functions of ϕ, θ/T, e and β as detailed in Appendix B. It can be verified that

$$\mu_r \to 0 \quad \text{as} \quad \phi \to 0, \tag{2.17}$$

i.e. the vortex viscosity is identically zero in a dilute granular gas, and hence the additional contribution to the stress tensor (in (2.14)) vanishes in the dilute limit. Therefore, the stress tensor for a system of rough particles is symmetric in the Boltzmann limit ($\phi \to 0$), and its asymmetry is a consequence of the Enskog-level correction ($\phi \neq 0$) to transport coefficients. We note that this stress-asymmetry appears at the Navier–Stokes-order of approximation.

At the Navier–Stokes-order of approximation, both the kinetic and collisional components of the couple stress are zero, i.e.

$$\boldsymbol{G} = \boldsymbol{G}_{kin} + \boldsymbol{G}_{col} = 0. \tag{2.18}$$

This has been verified in MD simulations of the uniform shear flow of rough granular materials (Campbell 1993; Lun & Bent 1994). Only at the Burnett-order approximation, do we obtain non-zero contributions to the couple stress. We note in passing that the couple stresses play an important role on the dynamics of the flow near the boundaries, with the bulk quantities remaining relatively unaffected, as confirmed by the MD simulations of bounded Couette flow (Campbell 1993) and of inclined chute flow (Mitarai *et al.* 2002). Since the present work is devoted to unbounded shear flow, we do not consider any boundary effect (see, last paragraph in § 8) and hence the couple stress $\boldsymbol{G}$ is set to zero in the present analysis (refer to equations (2.11) and (2.13)).

The constitutive expression for the angular momentum source, $\boldsymbol{\Psi}$, is given by:

$$\boldsymbol{\Psi} = -2\mu_r(2\boldsymbol{\Omega} - \nabla \times \boldsymbol{u}). \tag{2.19}$$

It is clear that the transfer of angular momentum arises if the spin velocity differs from the mean vorticity of the flow, i.e. if $\boldsymbol{\Omega} \neq (1/2)\nabla \times \boldsymbol{u}$.

https://doi.org/10.1017/S002211200600214X Published online by Cambridge University Press

The translational ($\boldsymbol{q}$) and rotational ($\boldsymbol{q}_r$) heat fluxes can be written in a generalized Fourier form:

$$\boldsymbol{q} = -\kappa \nabla T - \kappa_h \nabla \theta, \tag{2.20}$$

$$\boldsymbol{q}_r = -\kappa_r \nabla T - \kappa_{rh} \nabla \theta, \tag{2.21}$$

where the translational and rotational 'pseudothermal' conductivities κ, κ_h, κ_r and κ_{rh} are

$$\left.\begin{aligned} \kappa &= \rho_p \sigma T^{1/2} f_4(\phi, \theta/T; e, \beta, K), & \kappa_h &= \rho_p \sigma T^{1/2} f_{4h}(\phi, \theta/T; e, \beta, K), \\ \kappa_r &= \rho_p \sigma T^{1/2} f_{4r}(\phi, \theta/T; e, \beta, K), & \kappa_{rh} &= \rho_p \sigma T^{1/2} f_{4rh}(\phi, \theta/T; e, \beta, K), \end{aligned}\right\} \tag{2.22}$$

and the rate of dissipation of translational ($\mathscr{D}$) and rotational ($\mathscr{D}_r$) kinetic energy (per unit volume) are given by:

$$\mathscr{D} = \frac{\rho_p}{\sigma} T^{3/2} f_5(\phi, \theta/T; e, \beta, K), \tag{2.23}$$

$$\mathscr{D}_r = -\frac{\rho_p}{\sigma} T^{3/2} f_{5r}(\phi, \theta/T; \beta, K), \tag{2.24}$$

where the expressions for $f_{4i}(\cdot)$ and $f_{5i}(\cdot)$ are provided in Appendix B.

For the Enskog-corrected transport coefficients, we need an expression for the radial distribution function which is taken to be that of Carnahan and Starling:

$$\chi(\phi) = \frac{(1 - \phi/2)}{(1 - \phi)^3}, \tag{2.25}$$

that diverges as $\phi \to 1$. Another well-known functional form for $\chi(\phi)$ is

$$\chi(\phi) = \frac{1}{1 - (\phi/\phi_{max})^{1/3}}, \tag{2.26}$$

that diverges in the limit $\phi \to \phi_{max}$, where $\phi_{max} = 0.65$ for the random close-packing limit for spheres. Both (2.25) and (2.26) will be used to check the dependence of stability properties on $\chi(\phi)$.

3. Non-dimensional equations and the base state

3.1. *Non-dimensional equations of motion*

We have non-dimensionalized all quantities via the following scaling:

$$\left.\begin{aligned} \boldsymbol{x}^* &= \frac{\boldsymbol{x}}{\sigma}, \quad t^* = \dot{\gamma} t, \quad \boldsymbol{u}^* = \frac{\boldsymbol{u}}{\sigma \dot{\gamma}}, \quad \boldsymbol{\Omega}^* = \frac{\boldsymbol{\Omega}}{\dot{\gamma}}, \quad T^* = \frac{T}{\sigma^2 \dot{\gamma}^2}, \\ \theta^* &= \frac{\theta}{\sigma^2 \dot{\gamma}^2}, \quad \boldsymbol{P}^* = \frac{\boldsymbol{P}}{\rho_p \sigma^2 \dot{\gamma}^2}, \quad \boldsymbol{\Psi}^* = \frac{\boldsymbol{\Psi}}{\rho_p \sigma^2 \dot{\gamma}^2}, \\ (\boldsymbol{q}^*, \boldsymbol{q}_r^*) &= \frac{1}{\rho_p \sigma^3 \dot{\gamma}^3} (\boldsymbol{q}, \boldsymbol{q}_r), \quad (\mathscr{D}^*, \mathscr{D}_r^*) = \frac{1}{\rho_p \sigma^2 \dot{\gamma}^3} (\mathscr{D}, \mathscr{D}_r), \end{aligned}\right\} \tag{3.1}$$

where $\dot{\gamma}$ is the shear rate. Here onward, for convenience, we will omit the starred-superscript and denote non-dimensional quantities by their bare counterparts. The resulting non-dimensional equations in the absence of body force and body couple

https://doi.org/10.1017/S0022112006002140X Published online by Cambridge University Press

take the following form:

$$\left.\begin{aligned}
\frac{\partial \phi}{\partial t} + \nabla\cdot(\phi \boldsymbol{u}) &= 0,\\
\phi\left(\frac{\partial}{\partial t} + \boldsymbol{u}\cdot\nabla\right)\boldsymbol{u} &= -\nabla\cdot\boldsymbol{P},\\
\tfrac{1}{4}K\phi\left(\frac{\partial}{\partial t} + \boldsymbol{u}\cdot\nabla\right)\boldsymbol{\Omega} &= \boldsymbol{\Psi},\\
\tfrac{3}{2}\phi\left(\frac{\partial}{\partial t} + \boldsymbol{u}\cdot\nabla\right)T &= -\nabla\cdot\boldsymbol{q} - \boldsymbol{P}:\nabla\boldsymbol{u} - \mathscr{D},\\
\tfrac{3}{2}\phi\left(\frac{\partial}{\partial t} + \boldsymbol{u}\cdot\nabla\right)\theta &= -\nabla\cdot\boldsymbol{q}_r - \mathscr{D}_r - \boldsymbol{\Omega}\cdot\boldsymbol{\Psi}.
\end{aligned}\right\} \tag{3.2}$$

The non-dimensional forms of the stress tensor $\boldsymbol{P}$, the angular momentum source $\boldsymbol{\Psi}$, the translational and rotational heat fluxes, $\boldsymbol{q}$ and $\boldsymbol{q}_r$, respectively, are the same as in (2.14) and (2.19)–(2.21), with the associated non-dimensional transport coefficients having the following forms:

$$\left.\begin{aligned}
p(\phi,T) &= T f_1(\phi), & \mu(\phi,T,\theta) &= \sqrt{T} f_2(\phi,\theta/T),\\
\mu_r(\phi,T) &= \sqrt{T} f_{2r}(\phi), & \xi(\phi,T) &= \sqrt{T} f_3(\phi),\\
\kappa(\phi,T,\theta) &= \sqrt{T} f_4(\phi,\theta/T), & \kappa_h(\phi,T,\theta) &= \sqrt{T} f_{4h}(\phi,\theta/T),\\
\kappa_r(\phi,T,\theta) &= \sqrt{T} f_{4r}(\phi,\theta/T), & \kappa_{rh}(\phi,T,\theta) &= \sqrt{T} f_{4rh}(\phi,\theta/T),\\
\mathscr{D}(\phi,T,\theta) &= T^{3/2} f_5(\phi,\theta/T), & \mathscr{D}_r(\phi,T,\theta) &= -T^{3/2} f_{5r}(\phi,\theta/T).
\end{aligned}\right\} \tag{3.3}$$

3.2. *Base state: uniform shear flow and energy non-equipartition*

We consider the three-dimensional unbounded shear flow of a micropolar granular fluid in the absence of gravity, with the streamwise, transverse and spanwise coordinate axes being denoted by x, y and z, respectively. The base state is steady ($\partial/\partial t(\cdot) = $) and fully developed ($\partial/\partial x(\cdot) = 0$), having no variation in the spanwise direction. For this case, the mass balance equation, the x- and z-components of the linear momentum equations and the x- and y-components of the angular momentum equations are identically satisfied. The only non-zero velocity field is the streamwise velocity which varies linearly with y, with constant density and granular temperatures throughout the flow field. Thus, the base-state hydrodynamic fields are given by

$$\left.\begin{aligned}
\phi^0 &= \text{constant},\\
\boldsymbol{u}^0 &\equiv \left(u_1^0, u_2^0, u_3^0\right)^T = \left(u_{1y}^0 y, 0, 0\right)^T,\\
\boldsymbol{\Omega}^0 &\equiv \left(\Omega_1^0, \Omega_2^0, \Omega_3^0\right)^T = \left(0, 0, -u_{1y}^0/2\right)^T,\\
T^0 &\equiv T^0(\phi^0, e, \beta) = \text{constant},\\
\theta^0 &\equiv \theta^0(\phi^0, e, \beta) = \text{constant}.
\end{aligned}\right\} \tag{3.4}$$

where u_{1y}^0 is the non-dimensional shear rate. The base-state fields are denoted by a superscript '0', and the subscripts 1, 2 and 3 to the velocity fields refer to their components in the x, y and z directions, respectively. We will analyse the stability characteristics of this uniform-shear base flow (3.4).

The base-state spin-velocity field, $\boldsymbol{\Omega}^0$, is obtained from the balance equation of angular momentum:

$$\begin{aligned}
&\boldsymbol{\Psi}^0 = 0 = (2\boldsymbol{\Omega}^0 - \nabla\times\boldsymbol{u}^0)\\
\Rightarrow\ &\boldsymbol{\Omega}^0 = \tfrac{1}{2}\left(0, 0, -u_{1y}^0\right)^T = \left(\Omega_1^0, \Omega_2^0, \Omega_3^0\right)^T.
\end{aligned} \tag{3.5}$$

https://doi.org/10.1017/S002211200600214X Published online by Cambridge University Press

Thus, the mean spin velocity is equal to the rate of 'rotational' bulk deformation (i.e. the mean vorticity), and, as a consequence, the stress tensor for the uniform-shear base flow remains symmetric. Equation (3.5), together with the balance equation of rotational granular energy, yields an expression for the ratio between θ^0 and T^0:

$$\mathscr{D}_r^0 = 0 = -T^{0^{3/2}} f_{5r}^0, \qquad \Rightarrow \frac{\theta^0}{T^0} = \frac{\eta_2}{(1-\eta_2/K)}, \tag{3.6}$$

where $\eta_2 = (1+\beta)K/2(1+K)$. If the translational and the rotational granular temperatures are equally partitioned (i.e. $T^0 = \theta^0$), then it follows that $\beta \equiv 1$ which corresponds to perfectly rough particles. The other extreme of perfectly smooth particles ($\beta = -1$) yields $\theta^0 = 0$, i.e. all the energies are contained in the translational degrees of freedom (see figure 2*a* of McNamara & Luding 1998). Thus, under general conditions ($-1 < \beta < 1$), the equipartition principle does not hold for a sheared granular system. It is worth mentioning that the above temperature ratio has been tested in MD simulations of shear flow (McNamara & Luding 1998), with the collision model being the same as discussed in § 2.1. They found almost perfect agreement between simulation and theory (see their figure 2*a*) for the whole range of $\beta \in (-1, 1)$. They also reported similar levels of agreement between simulation and theory for the vertically vibrated system as well as for the freely cooling system of rough particles.

An expression for T^0 can be obtained by equating the production term due to the shear-work ($-\boldsymbol{P}^0 : \nabla \boldsymbol{u}^0$) with the collisional dissipation term ($\mathscr{D}^0$) in the balance equation for the translational granular energy:

$$T^0 = u_{1y}^{0\,2} \frac{f_2(\phi^0, \theta^0/T^0; e, \beta, K)}{f_5(\phi^0, \theta^0/T^0; e, \beta, K)}. \tag{3.7}$$

Note that by specifying volume fraction of the base flow (ϕ^0) and the two restitution coefficients (e and β), the base-state fields are completely determined.

4. Linear stability analysis via Kelvin decomposition

To perform the linear stability analysis, we decompose each field variable as the sum of its mean (denoted by a superscript '0') and a small perturbation (denoted by a prime), with the mean corresponding to the base flow (3.4): $\phi(x, y, z, t) = \phi^0 + \phi'(x, y, z, t)$, etc. For example, the linearized form of the perturbation stress tensor is given by

$$\boldsymbol{P}' = [p' - \xi^0(\nabla \cdot \boldsymbol{u}')]\mathbf{1} - 2\mu^0 \boldsymbol{S}' - 2\mu' \boldsymbol{S}^0 - \mu_r^0 \mathbf{1} \times (2\boldsymbol{\Omega}' - \nabla \times \boldsymbol{u}'), \tag{4.1}$$

with

$$\boldsymbol{S}' = \tfrac{1}{2}(\nabla \boldsymbol{u}' + (\nabla \boldsymbol{u}')^T) - \tfrac{1}{3}(\nabla \cdot \boldsymbol{u}')\mathbf{1}.$$

Note that even though the stress tensor for the present base flow is symmetric, the perturbation stress tensor remains asymmetric since $\boldsymbol{\Omega}' \neq (1/2)\nabla \times \boldsymbol{u}'$ (i.e. the perturbation angular momentum source is non-zero). The perturbations in pressure, shear and vortex viscosities are

$$p' = p_\phi^0 \phi' + p_T^0 T', \quad \mu' = \mu_\phi^0 \phi' + \mu_T^0 T' + \mu_\theta^0 \theta', \quad \mu_r' = \mu_{r\phi}^0 \phi' + \mu_{rT}^0 T', \tag{4.2}$$

where the subscripts ϕ, T and θ denote the respective partial derivatives, evaluated at base-state conditions. The linearized forms of $\boldsymbol{\Psi}'$, $\boldsymbol{q}'$, $\boldsymbol{q}_r'$, $\mathscr{D}'$ and $\mathscr{D}_r'$ are obtained in a similar fashion.

https://doi.org/10.1017/S0022112006002144X Published online by Cambridge University Press

Substituting the above perturbation flux quantities into the governing equations and linearizing about the base-state, we obtain a set of linear partial differential equations for the perturbation variables, $\boldsymbol{X} = (\phi', u_1', u_2', u_3', \Omega_1', \Omega_2', \Omega_3', T', \theta')^T$:

$$\left(\frac{\partial}{\partial t} + u_1^0 \frac{\partial}{\partial x}\right) \boldsymbol{X} = \mathscr{L}(\nabla, \nabla^2)\boldsymbol{X}, \tag{4.3}$$

where $\mathscr{L}(\cdot)$ represents the linear stability operator whose explicit form is omitted. Since the coefficients in (4.3) are constants except in the convective term ($u_1^0 \partial/\partial x(\cdot) \equiv y\partial/\partial x(\cdot)$), the linear stability equation (4.3) is not invariant under translation along the transverse direction (y), and hence we cannot seek normal-mode solutions, via Fourier decomposition, along y. Following Kelvin (1887), however, it can be shown that these equations (4.3) admit special time-dependent normal-mode solutions of the following form:

$$\boldsymbol{X}(\boldsymbol{x}, t) = \widehat{\boldsymbol{X}}(t) \exp[\mathrm{i}\boldsymbol{k}(t) \cdot \boldsymbol{x}], \tag{4.4}$$

where

$$\left.\begin{aligned} \boldsymbol{X}(\boldsymbol{x}, t) &= [\phi', u_1', u_2', u_3', \Omega_1', \Omega_2', \Omega_3', T', \theta'](\boldsymbol{x}, t), \\ \widehat{\boldsymbol{X}}(t) &= [\widehat{\phi}, \widehat{u}_1, \widehat{u}_2, \widehat{u}_3, \widehat{\Omega}_1, \widehat{\Omega}_2, \widehat{\Omega}_3, \widehat{T}, \widehat{\theta}](t), \\ \boldsymbol{k}(t) &= [k_x, k_y - k_x t, k_z]. \end{aligned}\right\} \tag{4.5}$$

Note that the y-component of the wavevector

$$k_y(t) \equiv k_y - k_x t \tag{4.6}$$

changes with time, and consequently the wavevector $\boldsymbol{k}(t)$ is turned in the clockwise direction by the mean shear field. This time-dependence of the wavevector, $\boldsymbol{k}(t)$, arises solely from the special base flow (i.e. the 'uniform' shear field). Substituting (4.4) into the linearized stability equation (4.3), we obtain a set of nine ordinary differential equations:

$$\frac{\mathrm{d}\widehat{\boldsymbol{X}}}{\mathrm{d}t} = \mathscr{A}(t)\widehat{\boldsymbol{X}} \tag{4.7}$$

where the time-dependent 9×9-matrix, $\mathscr{A}(t)$, has a quadratic-dependence on time:

$$\mathscr{A}(t) \equiv \mathscr{L}(\mathrm{i}\boldsymbol{k}, \mathrm{i}^2\boldsymbol{k}^2) = \mathscr{A}_0 + \mathscr{A}_1 t + \mathscr{A}_2 t^2. \tag{4.8}$$

The elements of $\mathscr{A}(t)$ are given in Appendix C.

4.1. *Control parameters*

Recall that the base flow is completely specified by specifying the solid fraction of particles ϕ^0, the coefficient of normal restitution e, the coefficient of tangential restitution β and the non-dimensional moment of inertia K. The shear rate u_{1y}^0 does not enter into the stability problem since it has been scaled out ($u_{1y}^0 = 1$) owing to our adopted scaling for non-dimensionalization. There are three stability parameters in the form of the streamwise (k_x), the transverse (k_y) and the spanwise (k_z) wavenumbers. Below we present the stability results for the Carnahan–Starling radial distribution function (2.25), and the consequence of using a different radial distribution function (2.26) is also discussed alongside.

5. Streamwise-independent perturbations ($k_x = 0$)

In this section, we present stability results for perturbations that do not vary along the streamwise direction, i.e. the streamwise wavenumber is zero ($k_x = 0$) for such

https://doi.org/10.1017/S002211200600214X Published online by Cambridge University Press

perturbations. For $k_x = 0$, it can be verified that $\mathscr{A}_1 = 0 = \mathscr{A}_2$ in (4.8). Since the stability matrix $\mathscr{A}$ is time-independent, we can look for 'exponential' solutions in time:

$$\widehat{\boldsymbol{X}}(t) = \widehat{\boldsymbol{X}}_0 \mathrm{e}^{\omega t}, \tag{5.1}$$

leading to an eigenvalue problem, where $\omega = \omega_r + \mathrm{i}\omega_i$, with ω_r denoting the growth/decay rate of perturbations and ω_i the frequency of perturbations. The flow is unstable, stable or neutrally stable for $\omega_r > 0$, < 0 and $= 0$, respectively. (This is the definition of 'exponential'/'asymptotic' instability.) Pure spanwise perturbations are treated in § 5.1, pure transverse perturbations in § 5.2, and the general case in § 5.3.

5.1. *Pure spanwise perturbations: an 'algebraic' instability*

Perturbations having variations only in the spanwise direction (i.e. $k_z \neq 0$, with $k_x = 0 = k_y$, i.e. the wave-vectors are aligned along the z-direction) are called pure spanwise perturbations. For this case, the equation for $\widehat{\Omega}_3$ is decoupled from the rest, with its solution

$$\widehat{\Omega}_3(t) = \widehat{\Omega}_3(0) \exp\left(-2c_k \mu_r^0 t\right), \tag{5.2}$$

that decays to zero as $t \to \infty$, representing a stable mode, and the decay rate is dictated by the vortex viscosity. The equations for $[\widehat{u}_1, \widehat{u}_2, \widehat{\Omega}_1, \widehat{\Omega}_2]$ are coupled:

$$\left.\begin{aligned} \frac{\mathrm{d}\widehat{u}_1}{\mathrm{d}t} &= -k_1\widehat{u}_1 + k_3\widehat{\Omega}_2 - u_{1y}^0\widehat{u}_2, & \frac{\mathrm{d}\widehat{u}_2}{\mathrm{d}t} &= -k_1\widehat{u}_2 - k_3\widehat{\Omega}_1, \\ \frac{\mathrm{d}\widehat{\Omega}_1}{\mathrm{d}t} &= k_4\widehat{u}_2 - k_2\widehat{\Omega}_1, & \frac{\mathrm{d}\widehat{\Omega}_2}{\mathrm{d}t} &= -k_4\widehat{u}_1 - k_2\widehat{\Omega}_2, \end{aligned}\right\} \tag{5.3}$$

where k_i are constants:

$$k_1 = c_p\left(\mu^0 + \mu_r^0\right)k_z^2, \quad k_2 = 2c_k\mu_r^0, \quad k_3 = -2\mathrm{i}c_p\mu_r^0 k_z, \quad k_4 = -\mathrm{i}c_k\mu_r^0 k_z, \tag{5.4}$$

with $c_p = 1/\phi^0$ and $c_k = 8/K\phi^0$. The second and third equations in (5.3) can be manipulated to yield a second-order differential equation for the transverse velocity $\widehat{u}_2$:

$$\frac{\mathrm{d}^2\widehat{u}_2}{\mathrm{d}t^2} + (k_1 + k_2)\frac{\mathrm{d}\widehat{u}_2}{\mathrm{d}t} + (k_1k_2 + k_3k_4)\widehat{u}_2 = 0, \tag{5.5}$$

with its solution being

$$\widehat{u}_2(t) = A_1\mathrm{e}^{m_1 t} + A_2\mathrm{e}^{m_2 t}, \tag{5.6}$$

where the exponents m_1 and m_2 are given by

$$m_{1,2} = \frac{(k_1 + k_2)}{2}\left[-1 \pm \sqrt{1 - \frac{4(k_1k_2 + k_3k_4)}{(k_1 + k_2)^2}}\right] \sim k_z^2. \tag{5.7}$$

Note that

$$(k_1k_2 + k_3k_4) = 2c_pc_k\mu^0\mu_r^0k_z^2 > 0,$$

implying that the real parts of both m_1 and m_2 are negative. Hence the transverse velocity decays with time, representing a stable mode. It is straightforward to verify that the decay rate of this mode increases with the inclusion of vortex viscosity in comparison to the case of perfectly smooth particles ($\beta = -1$). Substituting (5.6) into the second equation in (5.3), the solution for the streamwise spin-velocity can readily be obtained as:

$$\widehat{\Omega}_1(t) = -\frac{A_1(k_1 + m_1)}{k_3}\exp(m_1 t) - \frac{A_2(k_1 + m_2)}{k_3}\exp(m_2 t), \tag{5.8}$$

https://doi.org/10.1017/S002211200600214X Published online by Cambridge University Press

which also decays with time and hence is stable. Note that the constants of integration can be expressed in terms of $\widehat{u}_2(0)$ and $\widehat{\Omega}_1(0)$:

$$\left.\begin{aligned} A_1 &= -\frac{(k_1+m_2)}{(m_1-m_2)}\widehat{u}_2(0) - \frac{k_3}{(m_1-m_2)}\widehat{\Omega}_1(0), \\ A_2 &= \frac{(k_1+m_1)}{(m_1-m_2)}\widehat{u}_2(0) + \frac{k_3}{(m_1-m_2)}\widehat{\Omega}_1(0). \end{aligned}\right\} \tag{5.9}$$

It can be verified that the equation for the streamwise velocity $\widehat{u}_1$ satisfies a second-order differential equation,

$$\frac{\mathrm{d}^2\widehat{u}_1}{\mathrm{d}t^2} + (k_1+k_2)\frac{\mathrm{d}\widehat{u}_1}{\mathrm{d}t} + (k_1k_2+k_3k_4)\widehat{u}_1 = -u^0_{1y}\left[\frac{\mathrm{d}}{\mathrm{d}t} + k_2\right]\widehat{u}_2, \tag{5.10}$$

which is forced by the transverse velocity and its derivative via the mean shear-field (u^0_{1y}). The solution for $\widehat{u}_1$ is

$$\widehat{u}_1(t) = A_4\mathrm{e}^{m_1t} + A_5\mathrm{e}^{m_2t} + \underbrace{[A_6\mathrm{e}^{m_1t} + A_7\mathrm{e}^{m_2t}]t}, \tag{5.11}$$

where

$$\left.\begin{aligned} A_3 &= \left[\frac{(m_1+k_1)}{(2m_1+k_1+k_2)}A_1 + \frac{(m_2+k_1)}{(2m_2+k_1+k_2)}A_2\right]\frac{u^0_{1y}}{(m_1-m_2)}, \\ A_4 &= -\frac{(k_1+m_2)}{(m_1-m_2)}\widehat{u}_1(0) + \frac{k_3}{(m_1-m_2)}\widehat{\Omega}_2(0) - A_3, \\ A_5 &= \frac{(k_1+m_1)}{(m_1-m_2)}\widehat{u}_1(0) - \frac{k_3}{(m_1-m_2)}\widehat{\Omega}_2(0) + A_3, \\ A_6 &= -u^0_{1y}\left(\frac{m_1+k_2}{2m_1+k_1+k_2}\right)A_1, \quad A_7 = -u^0_{1y}\left(\frac{m_2+k_2}{2m_2+k_1+k_2}\right)A_2. \end{aligned}\right\} \tag{5.12}$$

It is clear that the streamwise velocity would also decay as $t \to \infty$, but, interestingly, grows for short times due to the 'under-braced' term in (5.11) that is linear in time. Note that this algebraic growth is driven by the forcing of $\widehat{u}_1(t)$ due to the transverse velocity $\widehat{u}_2(t)$ and the mean shear u^0_{1y} (see A_6 and A_7 in equation 5.12).

The solution to the transverse spin velocity is given by

$$\widehat{\Omega}_2(t) = A_8\mathrm{e}^{m_1t} + A_9\mathrm{e}^{m_2t} + \underbrace{(A_{10}\mathrm{e}^{m_1t} + A_{11}\mathrm{e}^{m_2t})t}, \tag{5.13}$$

where

$$\left.\begin{aligned} A_8 &= \frac{(m_1+k_1)}{k_3}\left[\frac{u^0_{1y}}{(2m_1+k_1+k_2)}A_1 + A_4\right], \; A_9 = \frac{(m_2+k_1)}{k_3}\left[\frac{u^0_{1y}}{(2m_2+k_1+k_2)}A_2 + A_5\right], \\ A_{10} &= \frac{(k_1+m_1)}{k_3}A_6, \qquad\qquad A_{11} = \frac{(k_1+m_2)}{k_3}A_7. \end{aligned}\right\} \tag{5.14}$$

Similar to streamwise velocity, the transverse spin velocity is also subjected to transient 'linear' growth due to the 'under-braced' term in (5.13).

https://doi.org/10.1017/S002211200600214X Published online by Cambridge University Press

To understand the origin of such short-time linear growth, we consider the inviscid stability equations (i.e. with $\mu = 0 = \mu_r$) whose solutions are

$$\left.\begin{aligned} \widehat{u}_1(t) &= \widehat{u}_1(0) + u^0_{1y}\widehat{u}_2(0)t, \quad & \widehat{u}_2(t) &= \widehat{u}_2(0), \\ \widehat{\Omega}_1(t) &= \widehat{\Omega}_1(0), & \widehat{\Omega}_2(t) &= \widehat{\Omega}_2(0). \end{aligned}\right\} \tag{5.15}$$

Clearly, $|\widehat{u}_1(t)| \to \infty$ as $t \to \infty$, and hence this is an algebraic instability (Ellingsen & Palm 1975) which is inviscid in nature. Note that this 'algebraic' instability grows linearly with time in contrast to the standard 'exponential' instability for which the perturbations grow/decay exponentially with time as in (5.1).

Figure 1 shows a set of results on the temporal evolutions of $\widehat{u}_1(t)$ and $\widehat{\Omega}_2(t)$ for the parameter values of $\phi = 0.1$ and $e = 0.99$, with the tangential restitution coefficient being set to (*a*, *b*) $\beta = -0.9$, (*c*, *d*) $\beta = 0$ and (*e*, *f*) $\beta = 0.9$. For all cases, the initial condition corresponds to $\widehat{u}_2(t = 0) = 1$, with null values for other fields at $t = 0$. It is observed that there is a substantial growth of the streamwise velocity, and the associated growth of the transverse spin velocity is smaller by about two orders of magnitude compared to that for $\widehat{u}_1(t)$. The initial growth of $\widehat{u}_1(t)$ closely follows the linear inviscid asymptote (5.15); the growth of $\widehat{\Omega}_2(t)$ lags behind that of $\widehat{u}_1(t)$ because the growth of the former is due to the growth of the latter. For both cases, however, the initial growth is arrested after some time by the viscosities of the granular fluid (μ^0 and μ^0_r) that eventually stabilize the flow. The maximum growth of $\widehat{u}_1(t)$ and $\widehat{\Omega}_2(t)$ decreases sharply with increasing value of the spanwise wavenumber k_z since the viscous decay rate ($\propto m_{1,2}$, see equation (5.7)) is proportional to k_z^2. Note that the peaks on the curves of $\widehat{u}_1(t)$ and $\widehat{\Omega}_2(t)$ occur at a time that is few orders of magnitude larger that the imposed shear rate. This time scale (which is proportional to k_z^{-2} and $(\mu^0 + \mu^0_r)^{-1}$), over which the above inviscid mechanism is active, decreases with increasing inelasticity as well as with increasing k_z.

It should be noted that even though the above time scale decreases with increasing inelasticity, our prediction of inviscid algebraic instability and the related momentum transfer mechanism (see below) hold for any value of inelasticity. This conclusion remains valid irrespective of whether we are using a Navier–Stokes'-level or a Burnett-level constitutive theory.

In physical terms, the above algebraic growth of $\widehat{u}_1(t)$ occurs owing to the transfer of momentum from the transverse velocity $\widehat{u}_2(0)$ via the mean shear field (u^0_{1y}), i.e. $\widehat{u}_2(0)$ extracts momentum from the mean shear (u^0_{1y}) and transfers it to $\widehat{u}_1(t)$. Note that the transverse spin velocity $\widehat{\Omega}_2(t)$ does not show any inviscid instability since it is neutrally stable in the inviscid limit. In fact, the algebraic growth of $\widehat{\Omega}_2(t)$ in (5.13) is due to its coupling with $\widehat{u}_1(t)$ via the vortex viscosity ($k_4 \propto \mu^0_r$). For this case, the vortex viscosity helps to extract streamwise momentum from $\widehat{u}_1(t)$ and transfers it to the rotational mode $\widehat{\Omega}_2(t)$. Based on this discussion, we propose the following route for the algebraic growth of $\widehat{u}_1(t)$ and $\widehat{\Omega}_2(t)$ in a sheared micropolar granular fluid:

Non-zero $\widehat{u}_2(0)$

$\Downarrow$ via inviscid 'algebraic' instability

Momentum transfer to $\widehat{u}_1(t)$

$\Downarrow$ via 'vortex' viscosity

Momentum transfer to $\widehat{\Omega}_2(t)$.

https://doi.org/10.1017/S002211200600214X Published online by Cambridge University Press

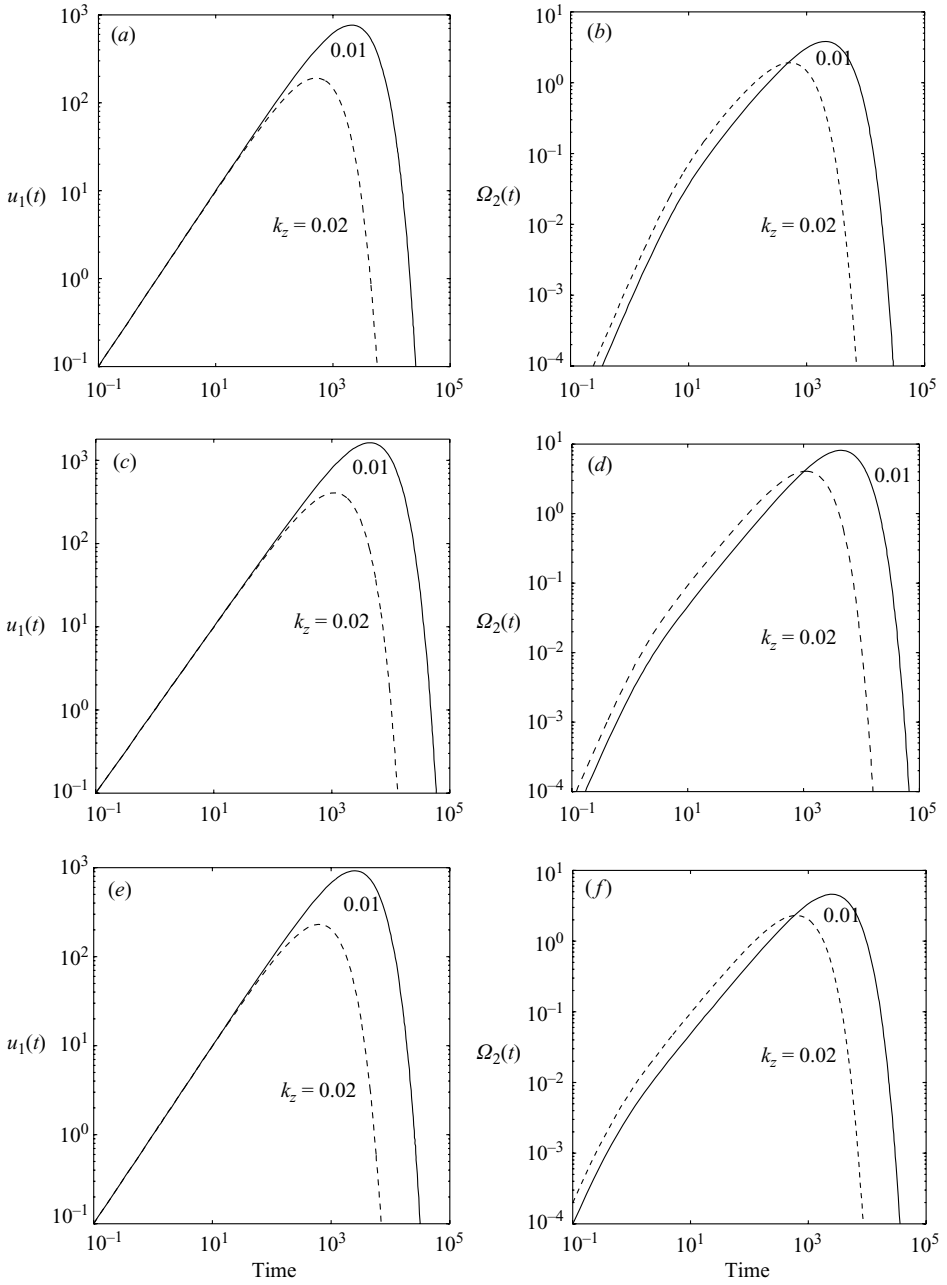


FIGURE 1. Evolutions of $\hat{u}_1(t)$ and $\hat{\Omega}_2(t)$ with time for $\phi = 0.1$ and $e = 0.99$: (a, b) $\beta = -0.9$; (c, d) $\beta = 0$; (e, f) $\beta = 0.9$. See text for other details.

Clearly, this is an 'instability-driven' momentum transfer mechanism from the translational degrees of freedom to the rotational degrees of freedom. Since we are driving the rotational field $\widehat{\Omega}_2(t)$ by an inviscid algebraic instability of $\widehat{u}_1(t)$, this can aptly be dubbed an *instability-induced rotational-driving* mechanism. Note that this is a purely three-dimensional effect since $k_z \neq 0$, and has no analogue in two-dimensional flows. One can control this momentum transfer mechanism by manipulating with

https://doi.org/10.1017/S002211200600214X Published online by Cambridge University Press

$\widehat{u}_2(0)$, k_z and the base-flow quantities (ϕ^0, T^0, θ^0, μ^0 and μ_r^0). This should be exploited in MD simulations for a better understanding of the underlying mechanism. Such simulations may also shed light on an important issue of controlling/manipulating the formation of instability-induced inhomogeneities in a sheared granular system by designing specific perturbations.

It is worth pointing out that the recent works on the stability of incompressible Newtonian fluids (Schmid & Henningson 2001, and references therein) have underscored the importance of 'algebraic' growth. There are many flow configurations (e.g. the plane Couette flow, pipe flow, etc.) that are stable according to the linear stability theory, but have been shown to have a finite critical Reynolds number in experiments. For such 'sub-critical' shear flows, the algebraic growth of perturbations leads to nonlinear states, in tune with experiments, via the 'bypass-transition' mechanism (Schmid & Henningson 2001). The possibility of a similar transition-mechanism in granular shear flows, that requires a nonlinear analysis, will be pursued in future.

5.1.1. *Dispersion relation for $\widehat{\phi}$, $\widehat{u}_3$, $\widehat{T}$ and $\widehat{\theta}$: long-wave scalings and 'exponential' instabilities*

The equations for the density $\widehat{\phi}$, spanwise velocity $\widehat{u}_3$, translational temperature $\widehat{T}$ and rotational temperature $\widehat{\theta}$ are coupled with each other, which lead to a fourth-order dispersion relation in ω:

$$\omega^4 + a_3\omega^3 + a_2\omega^2 + a_1\omega + a_0 = 0, \tag{5.16}$$

with the coefficients a_i having the following functional dependences with k_z:

$$\left.\begin{aligned} a_3 &= a_{30} + a_{32}k_z^2, & a_2 &= a_{20} + a_{22}k_z^2 + a_{24}k_z^4, \\ a_1 &= a_{12}k_z^2 + a_{14}k_z^4 + a_{16}k_z^6, & a_0 &= a_{02}k_z^2 + a_{04}k_z^4 + a_{06}k_z^6. \end{aligned}\right\} \tag{5.17}$$

The coefficients a_{ij} are real functions of e, β, K and the base-flow variables.

To determine the scalings of different modes with wavenumbers, we seek a long-wave expansion for ω in k_z,

$$\omega = \omega_0 + \omega_1 k_z + \omega_2 k_z^2 + \cdots.$$

The approximate solutions (with leading-order corrections) to all roots are

$$\left.\begin{aligned} \omega^{(1,2)} &= \omega_r \pm \mathrm{i}\omega_i, \\ \omega^{(3,4)} &= \omega_0 - \frac{\left[a_{02} + a_{12}\omega_0 + a_{22}\omega_0^2 + a_{32}\omega_0^3\right]k_z^2}{\omega_0\left[4\omega_0^2 + 3a_{30}\omega_0 + 2a_{20}\right]} + O\left(k_z^4\right) \end{aligned}\right\}, \tag{5.18}$$

where

$$\left.\begin{aligned} \omega_0 &= \frac{-a_{30} \mp \sqrt{a_{30}^2 - 4a_{20}}}{2}, \\ \omega_r &= \frac{-a_{12} + a_{30}a_{02}/a_{20}}{2a_{20}}k_z^2 + O\left(k_z^4\right), \\ \omega_i^2 &= -\frac{a_{02}}{a_{20}}k_z^2 + O\left(k_z^4\right). \end{aligned}\right\} \tag{5.19}$$

To zeroth-order in k_z, these roots are $\omega^{(1,2,3,4)} = (0, 0, \omega_0^-, \omega_0^+)$. Considering the smooth particle limit ($\beta \to -1$) we find that the real root $\omega^{(3)} = \omega_0^-$ degenerates to

$$\omega^{(3)} = \lim_{\beta\to-1} a_{30} = -\frac{2}{3\phi^0}f_5^0 T^{01/2} < 0,$$

https://doi.org/10.1017/S002211200600214X Published online by Cambridge University Press

	Exact values, (5.16)	Approximate values, (5.18)
$\omega^{(1)}$	$-1.2182028 \times 10^{-5} + \mathrm{i}1.338817 \times 10^{-3}$	$-1.2181 \times 10^{-5} + \mathrm{i}1.33883 \times 10^{-3}$
$\omega^{(2)}$	$-1.2182028 \times 10^{-5} - \mathrm{i}1.338817 \times 10^{-3}$	$-1.2181 \times 10^{-5} - \mathrm{i}1.33883 \times 10^{-3}$
$\omega^{(3)}$	$-4.853731728 \times 10^{-1}$	$-4.85373173 \times 10^{-1}$
$\omega^{(4)}$	$-2.71335954155 \times 10^{-1}$	$-2.71335954157 \times 10^{-1}$

TABLE 1. Comparison of approximate eigenvalues (5.18) with exact ones (5.16) for pure spanwise disturbances ($k_x = k_y = 0$): $\phi = 0.2$, $e = 0.9$, $\beta = -0.9$, $k_z = 0.001$.

	Exact values, (5.16)	Approximate values, (5.18)
$\omega^{(1)}$	$4.4558787633 \times 10^{-3}$	4.4525×10^{-3}
$\omega^{(2)}$	$-1.604556702 \times 10^{-1}$	$-1.60455671 \times 10^{-1}$
$\omega^{(3)}$	$-4.717291215 \times 10^{-1}$	-4.713×10^{-1}
$\omega^{(4)}$	$-2.867957579 \times 10^{-1}$	-2.86796×10^{-1}

TABLE 2. Comparison of approximate eigenvalues (5.18) with exact ones (5.16) for pure spanwise disturbances ($k_x = k_y = 0$): $\phi = 0.05$, $e = 0.9$, $\beta = -0.9$, $k_z = 0.001$.

which belongs to the decaying translational temperature mode, and the other real root $\omega^{(4)} = \omega_0^+$ to the rotational temperature; the complex conjugate pair belongs to density and spanwise velocity. Out of these four modes, the translational temperature is a fast mode since it decays faster than the rest.

The approximate values of $\omega^{(i)}$ are compared with their exact values (5.16) in table 1; parameters are set to $\phi = 0.2$, $e = 0.9$, $\beta = -0.9$, $k_z = 0.001$. The two real roots, along with the real parts of the two propagating modes, are negative. Decreasing the solid fraction to $\phi = 0.05$, we find that all four roots are real, as seen in table 2, with one of them being positive and hence unstable. In fact, the origin of this unstable mode can be traced to the complex conjugate pair ($\omega^{(1)}$ and $\omega^{(2)}$): the propagating modes merge together at a critical solid fraction to give birth to two stationary modes, one of which is unstable. Hence, the pure spanwise instability is stationary in nature as is the case for smooth particles (Wang *et al.* 1996); the inclusion of the rotational motion does not change the scaling of the unstable mode with k_z. (The details of the effects of rotational fields on the modal structure are omitted for the sake of brevity, but see the stability diagrams.)

Figure 2 shows four phase diagrams, delineating the zones of instability and stability, in the (ϕ, k_z)-plane for different values of the tangential restitution coefficient (*a*) $\beta = -1$, (*b*) -0.9, (*c*) 0 and (*d*) 1; the normal restitution coefficient is set to $e = 0.9$. In each panel, we have plotted the contours of the growth rate of the least stable mode,

$$\omega_r^l = \max \omega_r.$$

The flow is unstable inside the neutral stability contour (denoted by '0') and stable outside. For a given solid fraction (within the instability zone), the growth-rate of the least stable mode is zero at $k_z = 0$, increases with increasing k_z, reaches a maximum at some value of k_z and decreases monotonically thereafter. Compared to the case of smooth particles ($\beta = -1$) in figure 2(*a*), the size of the instability zone is maximum for $\beta = 0$ and minimum for $\beta = 1$ (see ordinates in figures 2*b*, 2*c* and 2*d*).

Figure 3 shows the same set of phase diagrams for the ideal case of rough particles with elastic collisions (i.e. $e = 1$ and $\beta \neq -1$). In the limit of perfectly smooth elastic particles ($\beta = -1$ and $e = 1$), the pure spanwise instability vanishes. Making the

https://doi.org/10.1017/S002211200600214X Published online by Cambridge University Press

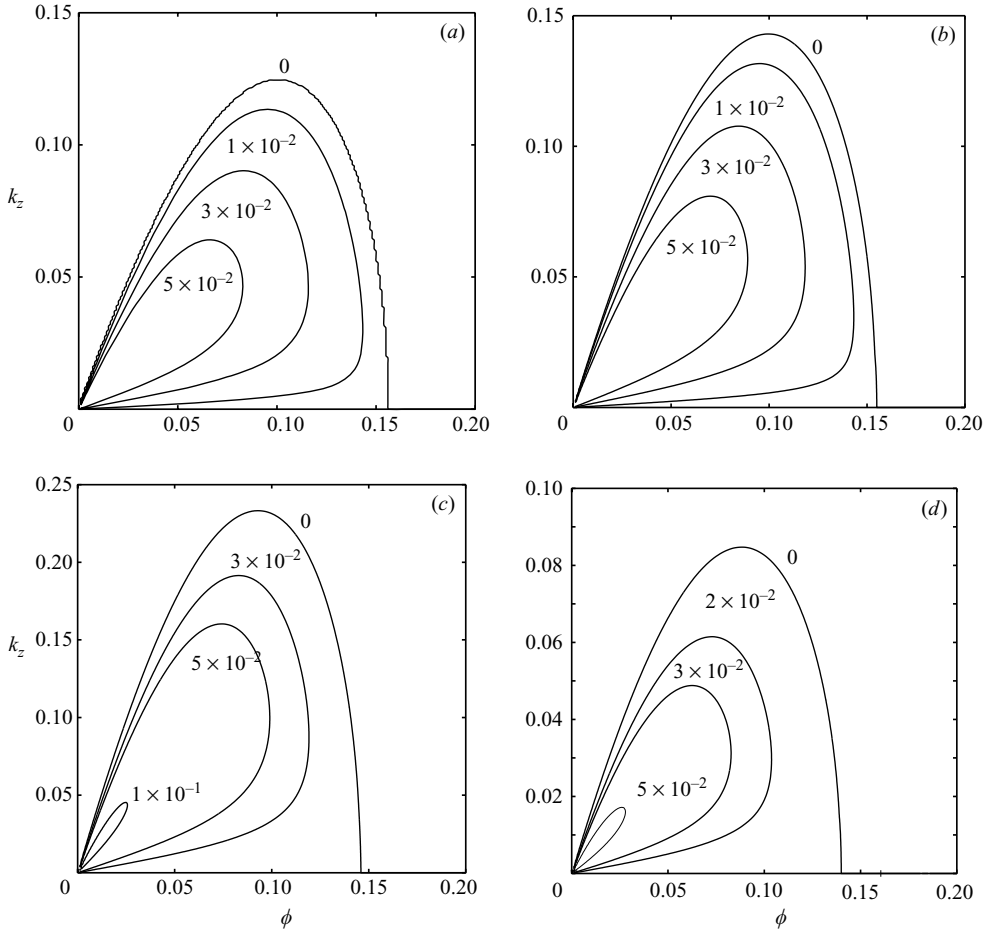


FIGURE 2. Stability maps in the (ϕ, k_z)-plane, showing the growth rate contours of the least stable eigenvalue, ω_r^l, for pure spanwise perturbations with inelastic particles $e = 0.9$: (*a*) $\beta = -1.0$; (*b*) $\beta = -0.9$; (*c*) $\beta = 0$; (*d*) $\beta = 1.0$.

particles slightly rough ($\beta = -0.9999$), this instability again appears in the (ϕ, k_z)-plane as observed in figure 3(*a*). As in the case of $e = 0.9$, the size of the instability zone is maximum for $\beta = 0$ (figure 3*c*). In figure 3(*d*), we have set $\beta = 0.9999$ for which the instability zone is very small and eventually shrinks to zero for perfectly rough particles ($\beta = 1$). Therefore, the pure spanwise instability survives even in the limit of perfectly elastic particles if $\beta \neq -1$ and 1.

The stationary nature ($\omega_i = 0$) of the pure spanwise instability helps to determine the locus of the neutral stability contour ($\omega_r = 0$) analytically by setting $\omega = 0$ in the dispersion relation (5.16), i.e. $a_0 = 0$, which is given by

$$k_z^2 = \frac{-a_{04} + \sqrt{a_{04}^2 - 4a_{06}a_{02}}}{2a_{06}}. \tag{5.20}$$

The critical solid fraction, $\phi \equiv \phi_c^s$, at which this instability sets in can be obtained by setting $k_z = 0$ in (5.20), and the maximum range of unstable spanwise wavenumber,

https://doi.org/10.1017/S0022112006002140X Published online by Cambridge University Press

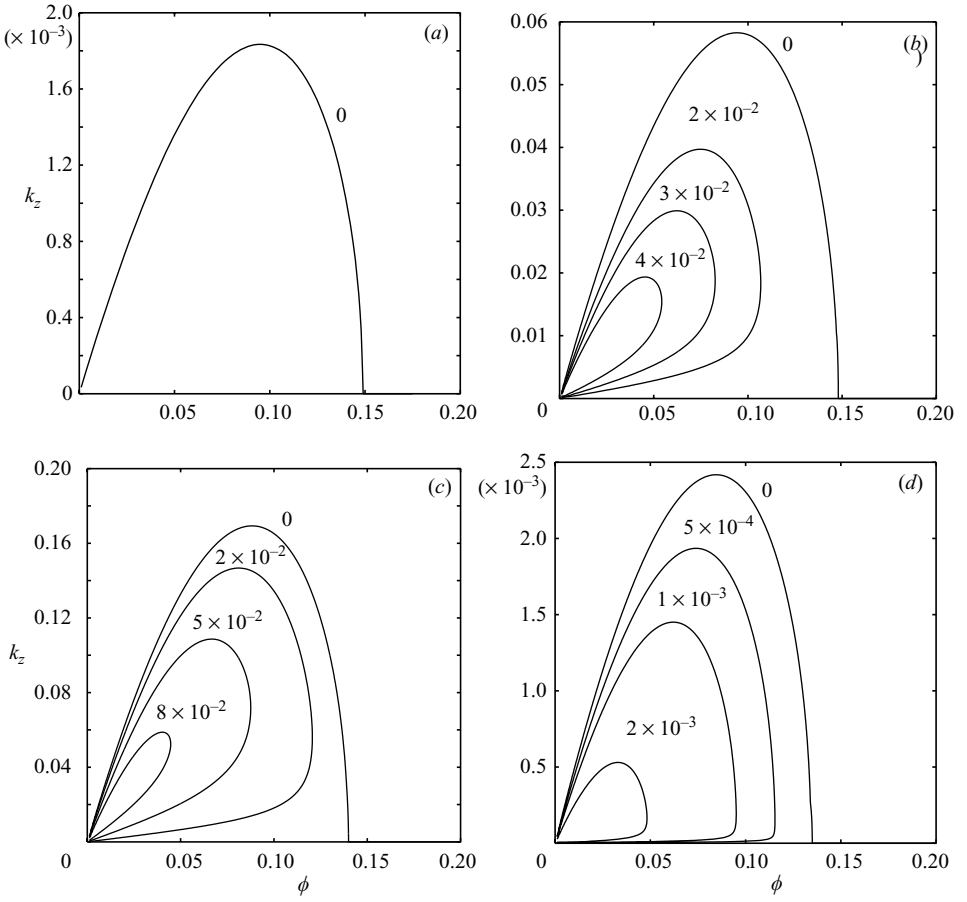


FIGURE 3. Same as in figure 2, but for particles with perfectly elastic collisions $e = 1.0$: (*a*) $\beta = -0.9999$; (*b*) $\beta = -0.9$; (*c*) $\beta = 0$; (*d*) $\beta = 0.9999$.

k_z^{max}, for this instability can be obtained by setting $\mathrm{d}k_z/\mathrm{d}\phi = 0$ in (5.20) (see figures 2 and 3).

The variations of the maximum growth rate of the spanwise unstable mode (maximized over all k_z and ϕ, see figures 2 and 3)

$$\omega_r^{max} = \sup_{k_z,\phi} \omega_r^l,$$

the maximum unstable spanwise wavenumber k_z^{max} and the critical solid fraction ϕ_c^s with the tangential restitution coefficient β are shown in figures 4(*a*), 4(*b*) and 4(*c*), respectively, for $e = 1.0$, 0.9 and 0.7. For the perfect elastic case ($e = 1$), both ω_r^{max} and k_z^{max} are zero for $\beta = -1$ and 1, and hence the flow is stable in these two limits. (The curves for $e = 0.999$ are indistinguishable from those for $e = 1$.) It is observed from figures 4(*a*) and 4(*b*) that the peaks in the curves of ω_r^{max} and k_z^{max} are located at $\beta > 0$ for $e = 1$, which shift to lower values of β as we decrease the normal restitution coefficient. From figure 4(*c*), we find that the critical solid fraction, ϕ_c^s, for spanwise instability decreases monotonically with increasing β for a given e; its value increases monotonically with decreasing e for any β. The dependence of ω_r^{max} on the choice

https://doi.org/10.1017/S0022112006002140X Published online by Cambridge University Press

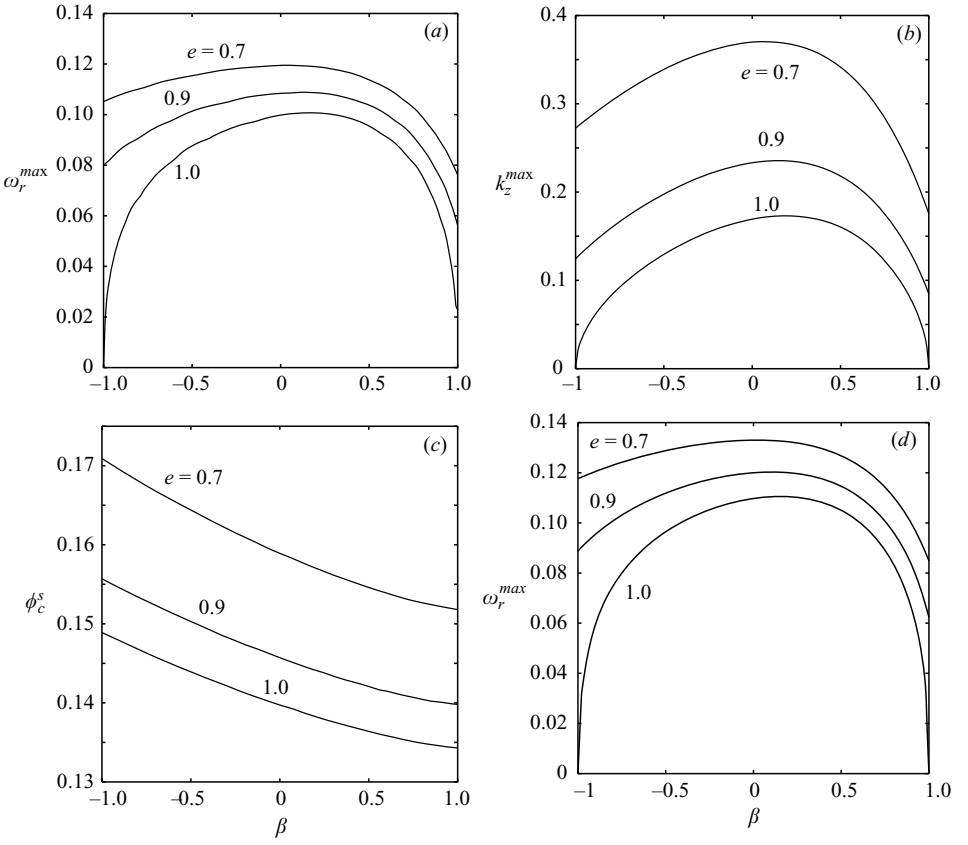


FIGURE 4. Variations of (*a*) ω_r^{max}, (*b*) k_z^{max} and (*c*) ϕ_c^s for pure spanwise perturbations with β for different e. (*d*) Same as (*a*), but for a different radial distribution function (2.26).

of the radial distribution function is shown in figure 4(*d*) for (2.26). The maximum growth rate (as well as k_z^{max}, not shown) is slightly larger for (2.26) in comparison with that for the Carnahan–Starling form (2.25); however, the critical solid fraction, ϕ_c^s, is slightly smaller (not shown) for (2.26).

5.2. *Pure transverse perturbations: long-wave scalings and 'exponential' instabilities*

Perturbations having variations only in the transverse direction (i.e. $k_y \neq 0$, with $k_x = 0 = k_z$, i.e. the wave-vectors are aligned along the y-direction) are called *pure transverse* perturbations. For this case, the equations for $\widehat{u}_3$, $\widehat{\Omega}_1$ and $\widehat{\Omega}_2$ are decoupled from the six rest equations, with solutions

$$\left.\begin{aligned} &\widehat{u}_3(t) = B_1 \exp(m_3 t) + B_2 \exp(m_4 t), \\ &\widehat{\Omega}_1(t) = B_3 \exp(m_3 t) + B_4 \exp(m_4 t) + B_5 \exp\left(-2c_k \mu_r^0 t\right), \ \ \widehat{\Omega}_2(t) = \Omega_2(0) \exp\left(-2c_k \mu_r^0 t\right), \end{aligned}\right\} \tag{5.21}$$

where B_1–B_5 are constants of integration whose explicit expressions are not shown for brevity. The exponents are given by

$$m_{3,4} = \frac{k_5 + k_8}{2} \pm \tfrac{1}{2}\sqrt{(k_5 + k_8)^2 + 4(k_6 k_7 - k_5 k_8)}, \tag{5.22}$$

https://doi.org/10.1017/S0022112006002140X Published online by Cambridge University Press

where

$$k_5 = -c_d\left(\mu^0 + \mu_r^0\right)k_y^2, \quad k_6 = -2\mathrm{i}c_p k_y, \quad k_7 = \mathrm{i}c_k\mu_r^0 k_y, \quad k_8 = -2c_k\mu_r^0.$$

Since $\mathrm{Re}\{m_{3,4}\} < 0$, all three modes decay with time, and hence are stable. For the six rest equations, the analysis boils down to that for pure transverse disturbances in two-dimensional flows. (For two-dimensional flows, there are two linear momentum equations for $\widehat{u}_1$ and $\widehat{u}_2$ and one angular momentum equation for $\widehat{\Omega}_3$, and hence we are left with six balance equations.) Seeking 'exponential' solutions for perturbation variables ($\sim \mathrm{e}^{\omega t}$), the dispersion relation can be obtained as:

$$\omega^6 + b_5\omega^5 + b_4\omega^4 + b_3\omega^3 + b_2\omega^2 + b_1\omega + b_0 = 0, \tag{5.23}$$

with the coefficients b_i having the following functional dependence with k_y:

$$\left.\begin{aligned} b_5 &= b_{50} + b_{52}k_y^2, & b_4 &= b_{40} + b_{42}k_y^2 + b_{44}k_y^4, \\ b_3 &= b_{30} + b_{32}k_y^2 + b_{34}k_y^4 + b_{36}k_y^6, & b_2 &= b_{22}k_y^2 + b_{24}k_y^4 + b_{26}k_y^6 + b_{28}k_y^8, \\ b_1 &= b_{12}k_y^2 + b_{14}k_y^4 + b_{16}k_y^6 + b_{18}k_y^8, & b_0 &= b_{04}k_y^4 + b_{06}k_y^6 + b_{08}k_y^8. \end{aligned}\right\} \tag{5.24}$$

The coefficients b_{ij} are real functions of e, β, K and the base-state variables.

Seeking a long-wave approximation for ω in k_y, we find that, to zeroth-order in k_y, there are three zero roots ($\omega_0^{(1)} = 0 = \omega_0^{(2)} = \omega_0^{(3)}$), and the other three roots are the solution of the following cubic polynomial:

$$\omega_0^3 + b_{50}\omega_0^2 + b_{40}\omega_0 + b_{30} = 0. \tag{5.25}$$

At this order, the smooth particle limit ($\beta \to -1$) yields $\omega_0^{(4,5,6)} = (\omega_{s0}, 0, 0)$, with

$$\omega_{s0} = \lim_{\beta\to -1} -b_{30} = -\frac{2}{3\phi^0} f_5^0 T^{01/2} < 0 \tag{5.26}$$

that corresponds to the decay-rate of the translational temperature; the other two roots, $\omega_0^{(5,6)}$, belong to $\widehat{\Omega}_3$ and $\widehat{\theta}$. As in the case of pure spanwise perturbations, the translational temperature remains the fast mode for pure transverse perturbations at this order.

With leading-order corrections in k_y, the approximations to all six roots are given by

$$\left.\begin{aligned} \omega^{(1)} &= -\frac{b_{04}}{b_{12}}k_y^2 + O\left(k_y^4\right), \\ \omega^{(2,3)} &= \omega_r \pm \mathrm{i}\omega_i, \\ \omega^{(4,5,6)} &= \omega_0 - \frac{b_{12} + b_{22}\omega_0 + b_{32}\omega_0^2 + b_{42}\omega_0^3 + b_{52}\omega_0^4}{\omega_0\left(3b_{30} + 4b_{40}\omega_0 + 5b_{50}\omega_0^2 + 6\omega_0^3\right)}k_y^2 + O\left(k_y^4\right), \end{aligned}\right\} \tag{5.27}$$

where the real and imaginary parts of $\omega^{(2,3)}$ are:

$$\left.\begin{aligned} \omega_r &= \frac{b_{04} + b_{40}\dfrac{b_{12}^2}{b_{30}^2} - b_{12}\dfrac{b_{22}}{b_{30}}}{2b_{12}}k_y^2 + O\left(k_y^4\right), \\ \omega_i^2 &= \frac{b_{12}}{b_{30}}k_y^2 + O\left(k_y^4\right). \end{aligned}\right\} \tag{5.28}$$

https://doi.org/10.1017/S002211200600214X Published online by Cambridge University Press

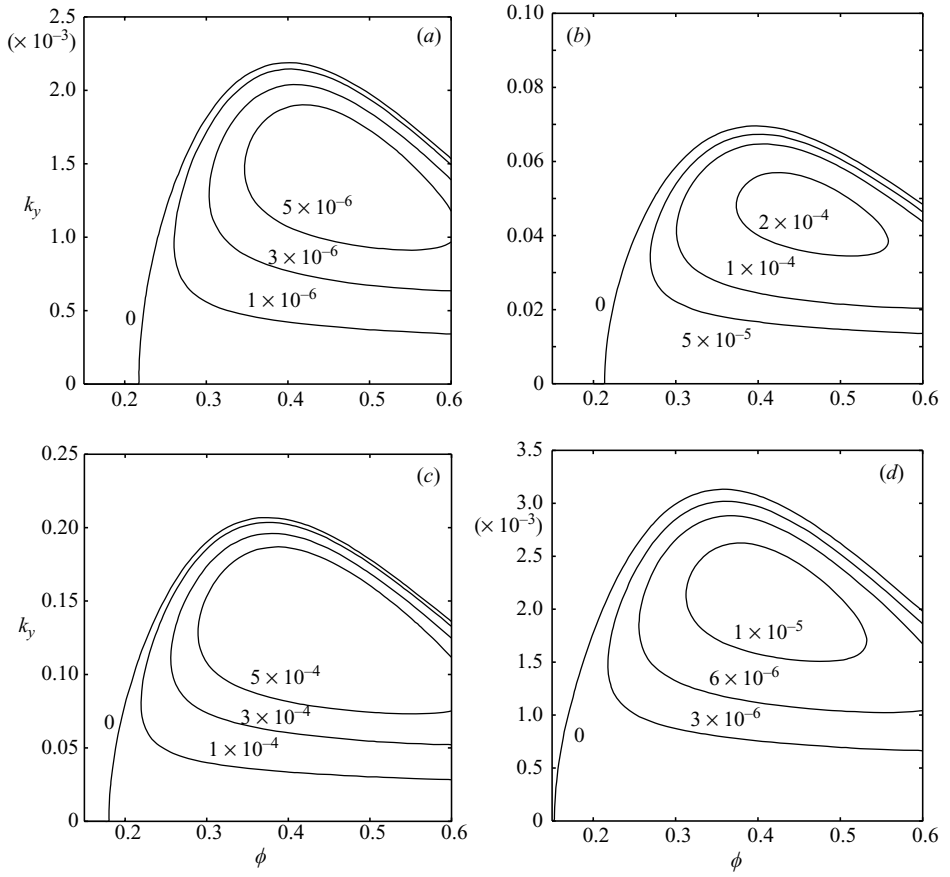


FIGURE 5. Same as in figure 3, but for pure transverse perturbations with $e = 1.0$.

Note that the leading-order corrections to two rotational modes vary quadratically with k_y, and they represent 'diffusive' modes and are stable. Comparisons of these approximate eigenvalues with their exact values (5.23) for different combinations of ϕ, e and β show excellent agreement for $k_y \leqslant 0.01$. In contrast to pure spanwise perturbations, the propagating modes for transverse perturbations remain stable for all ϕ, and the instability arises from one of the real roots, $\omega^{(1)}$, as in the case of smooth particles (Alam & Nott 1997, 1998), and hence is stationary in nature.

Figure 5 displays four phase diagrams in the (ϕ, k_y)-plane for a normal restitution coefficient of $e = 1.0$; the flow is unstable to pure transverse perturbations inside the neutral contour. It is observed that the pure transverse instability survives in the perfect elastic limit of rough particles, except for two extreme limits of $\beta = -1$ and 1. Increasing the value of β from -0.9999 (figure 5*a*) to -0.9 (figure 5*b*) increases the size of the unstable zone, but decreases beyond $\beta = 0$ (figure 5*c*). For a given roughness β, decreasing the value of e increases the size of the instability zone (not shown) as well as the growth rate of the least stable mode. Comparing figure 5 with figure 3, we find that the growth rate of the least stable mode is about two orders of magnitude smaller for pure transverse perturbations than that for pure spanwise perturbations.

https://doi.org/10.1017/S002211200600214X Published online by Cambridge University Press

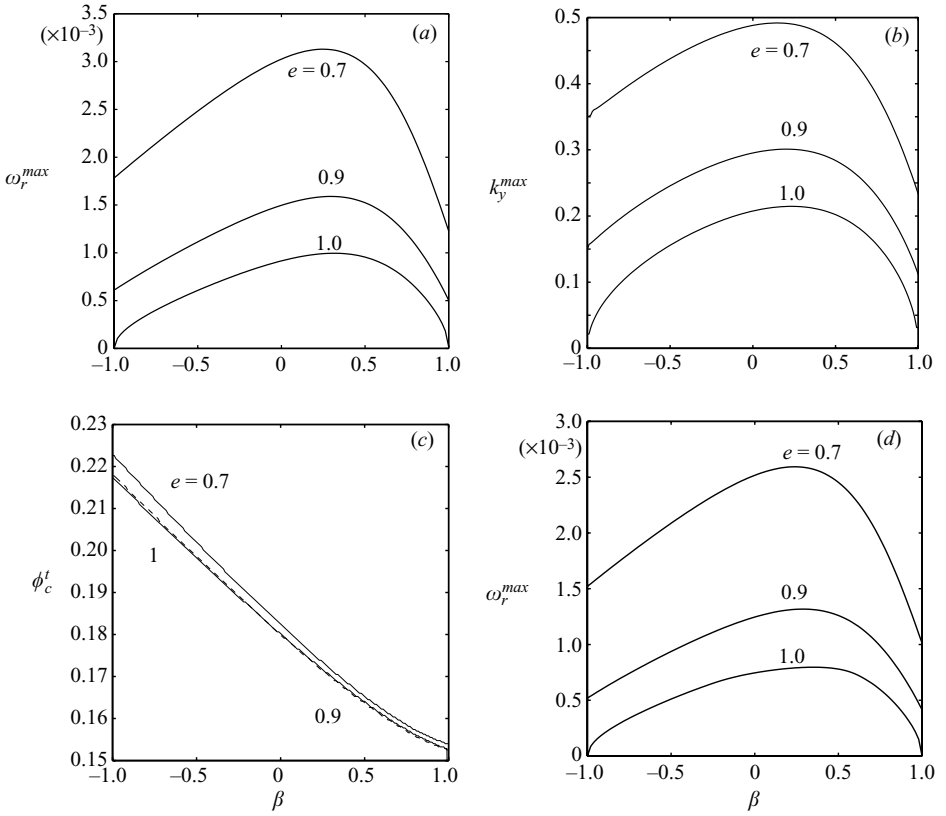


FIGURE 6. Variations of (*a*) ω_r^{max}, (*b*) k_y^{max} and (*c*) ϕ_c^t for pure transverse perturbations with β for different e. (*d*) Same as (*a*), but for a different radial distribution function (2.26).

In a phase diagram such as figure 5(*a*), the locus of the neutral contour ($\omega_r = 0$) can be analytically determined from

$$k_y^2 = \frac{-b_{06} + \sqrt{b_{06}^2 - 4b_{08}b_{04}}}{2b_{08}}. \tag{5.29}$$

The critical solid fraction, ϕ_c^t, for the onset of transverse instability is obtained from (5.29) by setting $k_y = 0$, and the maximum range of unstable transverse wavenumber, k_y^{max}, for this instability can be obtained by setting $\mathrm{d}k_y/\mathrm{d}\phi = 0$ in (5.29). The variations of the maximum growth rate of the transverse unstable mode (maximized over all k_y and ϕ, see figure 5)

$$\omega_r^{max} = \sup_{k_y,\phi} \omega_r^l,$$

the maximum unstable transverse wavenumber k_y^{max} and the critical solid fraction ϕ_c^t with β are shown in figures 6(*a*), 6(*b*) and 6(*c*), respectively. It is observed from figures 6(*a*) and 6(*b*) that the peaks in the curves of ω_r^{max} and k_y^{max} are located at $\beta > 0$ for $e = 1$, which shift to lower values of β as we decrease the value of e. The critical solid fraction, ϕ_c^t, for transverse instability decreases monotonically with increasing β for a given e as seen in figure 6(*c*), however, it does not vary much with e. The dependence of ω_r^{max} on the choice of the radial distribution function is shown in

https://doi.org/10.1017/S0022112006002140X Published online by Cambridge University Press

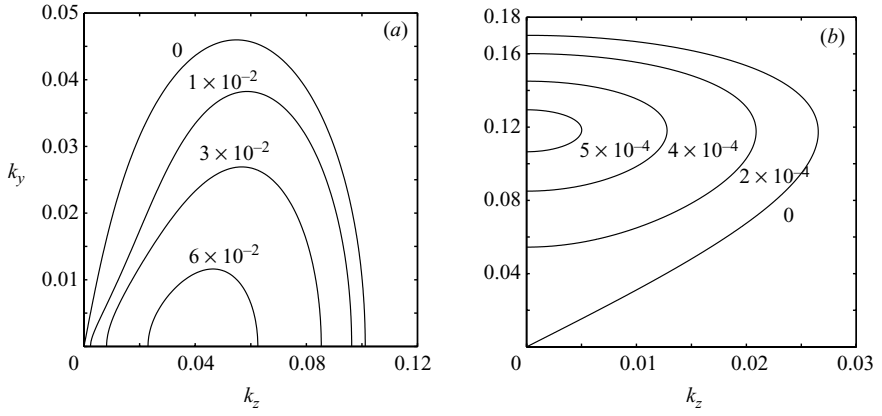


FIGURE 7. Stability maps in the (k_z, k_y)-plane, showing the growth rate contours of the least stable eigenvlaue, ω_r^l, for streamwise-independent perturbations with $e = 0.9$ and $\beta = -0.9$: (*a*) $\phi = 0.05$; (*b*) $\phi = 0.35$.

figure 6(*d*) for (2.26). The maximum growth rate (as well as k_y^{max}, not shown) is slightly smaller for (2.26) in comparison with that for (2.25).

Comparing figure 6(*c*) with figure 4(*c*), we find that for smooth particles ($\beta = -1$) there is a window of solid fractions, $\phi_c^s < \phi < \phi_c^t$, for which the flow is stable to both spanwise and transverse instabilities; the size of this window diminishes with increasing β, and at $e = 0.7$ the flow becomes unstable for all solid fractions if $\beta > 0.5$. (In fact, both spanwise and transverse instabilities coexist for a narrow window of solid fractions at $e = 0.7$ and $\beta > 0.5$, and the size of this window grows with decreasing e.)

5.3. *Perturbations with $k_y \neq 0$ and $k_z \neq 0$*

For the general case of streamwise-independent perturbations ($k_x = 0$), having modulations in both the transverse and spanwise directions ($k_y \neq 0$ and $k_z \neq 0$), the dispersion relation is a ninth-order polynomial that has been solved numerically.

Figure 7 shows two phase diagrams in the (k_z, k_y)-plane for solid fractions of $\phi = 0.05$ and 0.35; the restitution coefficients are set to $e = 0.9$ and $\beta = -0.9$. For both cases, the instabilities are stationary in nature, and their origin for dilute flows ($\phi = 0.05 \leqslant \phi_c^s$) can be traced back to the pure spanwise instability ($k_z \neq 0$) as discussed in § 5.1.1, and that for moderate-to-dense flows ($\phi = 0.35 \geqslant \phi_c^t$) to the pure transverse instability ($k_y \neq 0$) as discussed in § 5.2. The flow is unstable to non-zero values of k_y at long waves (figure 7*a*); in particular, the growth rate of the least stable mode is maximum at $k_y = 0$, and decreases monotonically with increasing k_y. For dense flows as in figure 7(*b*), the growth rate of the least stable mode is maximum at $k_z = 0$, and decreases monotonically with increasing k_z. For other values of β, the phase diagrams look similar to those in figure 7: the ranges of unstable k_y and k_z as well as the growth rate of the least stable mode reach maxima for intermediate values of β (> 0).

We had noted in §§ 5.1.1 and 5.2 that at large dissipations and $\beta > 0.5$, there is a range of solid fractions (around $\phi \sim 0.15$) for which both pure spanwise and pure transverse instabilities coexist; the maximum growth rate occurs at non-zero values of k_z for any k_y within this range of solid fractions. Therefore, we conclude that, for all values of β, the two-dimensional ($k_z = 0$) streamwise-independent perturbations

https://doi.org/10.1017/S002211200600214X Published online by Cambridge University Press

are more unstable than their three-dimensional counterparts if the solid fraction is larger than its critical value for pure spanwise instability (i.e. for $\phi > \phi_c^s$), while for $\phi < \phi_c^s$ the three-dimensional perturbations are the most unstable.

Lastly, a comment on the dependence of the observed instabilities on the system size is in order. The results presented in figures 2–7 suggest that the uniform shear flow is unstable if the wavenumber (which is inversely proportional to the system size) is small enough for a given β. This implies that these instabilities can be detected if the system size is large enough as is the case in MD simulations of shear flows (Hopkins, Louge & Jenkins 1993; Tan & Goldhirsch 1997). The effect of tangential restitution coefficient β on the 'critical' system size shows an interesting trend as can be ascertained from figures 4(b) and 6(b). It is observed that there is a critical $\beta_c \sim 0$ above/below which the critical system-size for the onset of these instabilities increases. Similar dependence on β holds for the instability growth rate as can be seen in figures 4(a) and 6(a). In summary, the maximum growth rate (ω_r^{max}) increases and the critical system size ($\propto k^{-1}$) for the instability-onset decreases if we make the particles slightly rough from the 'perfectly' smooth limit ($\beta = -1$) or slightly smoother from the 'perfectly' rough limit ($\beta = 1$).

6. General perturbations ($k_x, k_y, k_z \neq 0$)

6.1. *Long-time behaviour* ($t \to \infty$)

Here we consider general perturbations having variations in all three directions, i.e. for which

$$k_x, k_y, k_z \neq 0,$$

and analyse the temporal behaviour of $\hat{X}(t)$ in equation (4.7). Since the linear stability/instability corresponds to the asymptotic behaviour of the solutions of (4.7) in the limit of large time ($t \to \infty$), here we carry out an asymptotic analysis in the long-time limit. For large times ($t \gg 0$), the matrix $\mathscr{A}(t)$ in (4.7) can be approximated by its coefficient which is quadratic in time: $\mathscr{A}(t) \approx \mathscr{A}_2 t^2$, provided $\mathscr{A}_2$ has full rank. However, since $\mathscr{A}_2$ is rank-deficient, one has to be careful in determining the large-time behaviour of $\hat{X}(t)$. In this regard, we note that the earlier work of Schmid & Kytömaa (1994) was corrected in Alam & Nott (1997; personal communication, P. R. Nott 1996). We follow the above work to determine the large-time behaviour of $\hat{X}(t)$ by using the method of dominant balance (Bender & Orszag 1999).

The correct balance in the perturbation equations for the translational and rotational temperatures is between the time-derivative on the left-hand side and the corresponding quadratic term ($\propto t^2$) on the right-hand side. These two equations are coupled with each other and can be manipulated to yield two decoupled second-order differential equations for $\widehat{T}(t)$ and $\widehat{\theta}(t)$:

$$\left.\begin{aligned} \frac{\mathrm{d}^2\widehat{T}}{\mathrm{d}t^2} + \left[c_d\left(\kappa^0 + \kappa_{rh}^0\right)k_x^2 t^2 - \frac{2}{t}\right]\frac{\mathrm{d}\widehat{T}}{\mathrm{d}t} - \left[c_d\left(\kappa_r^0\kappa_h^0 - \kappa^0\kappa_{rh}^0\right)k_x^2\right]t^4\widehat{T} = 0, \\ \frac{\mathrm{d}^2\widehat{\theta}}{\mathrm{d}t^2} + \left[c_d\left(\kappa^0 + \kappa_{rh}^0\right)k_x^2 t^2 - \frac{2}{t}\right]\frac{\mathrm{d}\widehat{\theta}}{\mathrm{d}t} - \left[c_d\left(\kappa_r^0\kappa_h^0 - \kappa^0\kappa_{rh}^0\right)k_x^2\right]t^4\widehat{\theta} = 0. \end{aligned}\right\} \tag{6.1}$$

Using the following transformation for the independent variable:

$$\tau = t^3, \quad \frac{\mathrm{d}}{\mathrm{d}t} = 3t^2\frac{\mathrm{d}}{\mathrm{d}\tau}, \quad \frac{\mathrm{d}^2}{\mathrm{d}t^2} = 9t^4\frac{\mathrm{d}^2}{\mathrm{d}\tau^2} + \frac{2}{t}\frac{\mathrm{d}}{\mathrm{d}t}, \tag{6.2}$$

https://doi.org/10.1017/S0022112006002144X Published online by Cambridge University Press

the variable-coefficient equations (6.1) readily simplify to 'constant-coefficient' equations:

$$\left.\begin{aligned} 9\frac{\mathrm{d}^2\widehat{T}}{\mathrm{d}\tau^2} + 3\left[c_d\left(\kappa^0+\kappa^0_{rh}\right)k_x^2\right]\frac{\mathrm{d}\widehat{T}}{\mathrm{d}\tau} + \left[c_d\left(\kappa^0\kappa^0_{rh}-\kappa^0_r\kappa^0_h\right)k_x^2\right]\widehat{T} = 0,\\ 9\frac{\mathrm{d}^2\widehat{\theta}}{\mathrm{d}\tau^2} + 3\left[c_d\left(\kappa^0+\kappa^0_{rh}\right)k_x^2\right]\frac{\mathrm{d}\widehat{\theta}}{\mathrm{d}\tau} + \left[c_d\left(\kappa^0\kappa^0_{rh}-\kappa^0_r\kappa^0_h\right)k_x^2\right]\widehat{\theta} = 0. \end{aligned}\right\} \tag{6.3}$$

The solutions for $T(t)$ and $\theta(t)$ can be written in a compact form:

$$\frac{\widehat{T}(t)}{\widehat{T}(0)} = \frac{\widehat{\theta}(t)}{\widehat{\theta}(0)} = \frac{1}{(m_5-m_6)}[m_5\exp(m_5t^3) - m_6\exp(m_6t^3)], \tag{6.4}$$

where the exponents m_5 and m_6 are given by

$$m_{5,6} = \frac{c_d}{6}\left(\kappa^0+\kappa^0_{rh}\right)\left[-1 \pm \sqrt{1-\frac{4\left(\kappa^0\kappa^0_{rh}-\kappa^0_r\kappa^0_h\right)}{c_d\left(\kappa^0+\kappa^0_{rh}\right)^2k_x^2}}\right]k_x^2. \tag{6.5}$$

It is clear that the growth/decay rates of both $T(t)$ and $\theta(t)$ are the same.

From (6.5), we find that the exponent m_6 (or its real part) is always negative, and the instability is possible only if the other exponent m_5 is positive. Thus, for instability to occur, the term within the square root in (6.5) must be greater than one. This instability criterion simplifies to

$$\mathscr{F}(\phi, e, \beta) = \left(\kappa^0\kappa^0_{rh} - \kappa^0_r\kappa^0_h\right) < 0. \tag{6.6}$$

Considering the limit of nearly smooth particles (i.e. $\beta \approx -1$), it can be verified that

$$\kappa^0\kappa^0_{rh} = O(1+\beta), \quad \kappa^0_r\kappa^0_h = O((1+\beta)^2),$$

and hence $\mathscr{F}(\phi, e, \beta) = O(1+\beta) > 0$. The positivity of $\mathscr{F}$ has been verified numerically (not shown for brevity) for the whole range of β and other control parameters. Therefore, the exponent m_5 is negative for all parameter combinations. This implies that both the translational and rotational temperatures decay to zero as $t \to \infty$, representing stable modes.

It can be verified *a posteriori* that the dominant balance in the perturbation equations for $\widehat{u}_1$, $\widehat{u}_2$, $\widehat{u}_3$, $\widehat{\Omega}_1$, $\widehat{\Omega}_2$ and $\widehat{\Omega}_3$ is among the terms on the right-hand side of each equation; for example, the dominant balance for the $\widehat{u}_1$-momentum equation is:

$$c_1\widehat{\phi} + c_2\widehat{u}_1 + c_3\widehat{u}_2 + c_4\widehat{u}_3 + c_6\widehat{\Omega}_2 + c_7\widehat{\Omega}_3 = 0,$$

and that for the $\widehat{\Omega}_1$-momentum equation is

$$d_3\widehat{u}_2 + d_4\widehat{u}_3 + d_5\widehat{\Omega}_1 = 0,$$

where functional forms of c_i and d_i can be obtained from Appendix C. (Note that the terms associated with $\widehat{T}$ and $\widehat{\theta}$ are neglected in the dominant balance for the $\widehat{u}_1$-momentum equation since they are much smaller in magnitude (at large times) than those retained.) All these equations can be solved for $\widehat{u}_1$, $\widehat{u}_2$, $\widehat{u}_3$, $\widehat{\Omega}_1$, $\widehat{\Omega}_2$ and $\widehat{\Omega}_3$ in terms of $\widehat{\phi}$. Substituting the resulting expressions of $\widehat{u}_1$, $\widehat{u}_2$ and $\widehat{u}_3$ in the perturbation mass balance equation, the asymptotic expression for $\widehat{\phi}$ at large times can be derived as:

$$\widehat{\phi}(t) \sim \exp(-C_\phi t) \quad \text{with} \quad C_\phi = \frac{\phi^0 p_T^0}{(2\mu^0+\lambda^0)} > 0, \tag{6.7}$$

https://doi.org/10.1017/S002211200600214X Published online by Cambridge University Press

which decays as $t \to \infty$. The resulting leading-order expressions for the translational and rotational velocities are given by:

$$[\widehat{u}_1(t), \widehat{u}_2(t), \widehat{u}_3(t), \widehat{\Omega}_1(t), \widehat{\Omega}_2(t), \widehat{\Omega}_3(t)] \sim [t^{-1}, t^{-1}, t^{-2}, t^{-1}, t^{-1}, t^{0}] \exp(-C_\phi t), \quad (6.8)$$

which also decay as $t \to \infty$.

From the above analysis, we conclude that the unbounded granular shear flow of rough particles remains linearly stable to general perturbations with $k_x, k_y, k_z \neq 0$. This conclusion mirrors the previous work on the shear flow (Alam & Nott 1997) of perfectly smooth particles ($\beta = -1$).

6.2. *Short-time behaviour: initial growth rates*

In the short-time limit ($t \sim 0$), the stability matrix $\mathscr{A}(t)$ in (4.7) can be approximated by a constant matrix,

$$\mathscr{A}(t) \approx \mathscr{A}_0,$$

which allows standard 'exponential' solutions in time, leading to an eigenvalue problem

$$|\mathscr{A}_0 - \omega I| = 0.$$

It should be noted, however, that the growth rates obtained from such an analysis do not tell us anything about the long-time dynamics, but are estimates of the initial growth rates (Savage 1992; Babic 1993) of different modes (which would eventually decay as $t \to \infty$ as shown by the analysis in the above section). In this section, we use the term 'instability' to refer to modes having positive 'initial' growth rates.

Figures 8(*a*)–8(*c*) show three phase diagrams, delineating the zones of positive and negative initial growth rates, in the (k_z, k_y)-plane for tangential restitution coefficients of $\beta = -0.9$, 0 and 1, respectively, with $\phi = 0.05$ and $e = 0.9$; the streamwise wavenumber is set to $k_x = 0.01$. It is observed that the flow supports positive growth rates for a large range of k_y and k_z for all β; as in the case of pure spanwise and transverse instabilities, the size of the instability zone (for initial growth rates) is maximum for intermediate values of β. The kinks on the growth-rate contours in figures 8(*a*)–8(*c*) are a consequence of 'mode-crossings' which is evidenced in figure 8(*d*) where we have plotted the contours of ω_i (frequency) in the (k_z, k_y)-plane for the parameter set of figure 8(*a*); for a comparison, the corresponding neutral stability contour (denoted by a thick line) is also superimposed. It is clear from this figure that the phase diagram for $\beta = -0.9$ is composed of three different modes: the one for positive k_y and small k_z belongs to travelling waves (TW) as well as the small-lobe around $(k_z, k_y) = (0.07, -0.04)$, and the rest of the instability zone to stationary waves (SW). Increasing the tangential restitution coefficient to $\beta = 0$, one of the TW-lobes (for negative k_y) disappears from the (k_z, k_y)-plane, but reappears with further increase in β (see figure 8*c*).

In figure 8, the dominant TW/SW-mode (the one having the maximum initial growth rate for all k_y and k_z) comes from $k_z = 0$ modes for all values of β. Therefore, the two-dimensional perturbations are more unstable than their three-dimensional counterparts for all β with $k_x \neq 0$. The wavevector corresponding to the dominant TW mode 'opposes' the mean shear, but that for the dominant SW mode is along the mean shear.

Figure 9(*a*) shows a phase diagram for a moderately dense flow ($\phi = 0.35$), with other parameters as in figure 8(*a*). (The phase diagrams for $\phi = 0.2$ and $\phi = 0.5$ look similar to that for $\phi = 0.35$.) Looking at the frequency-contours of the least stable mode in figure 9(*b*), we find that there are two instability-lobes for TW, and one for

https://doi.org/10.1017/S002211200600214X Published online by Cambridge University Press

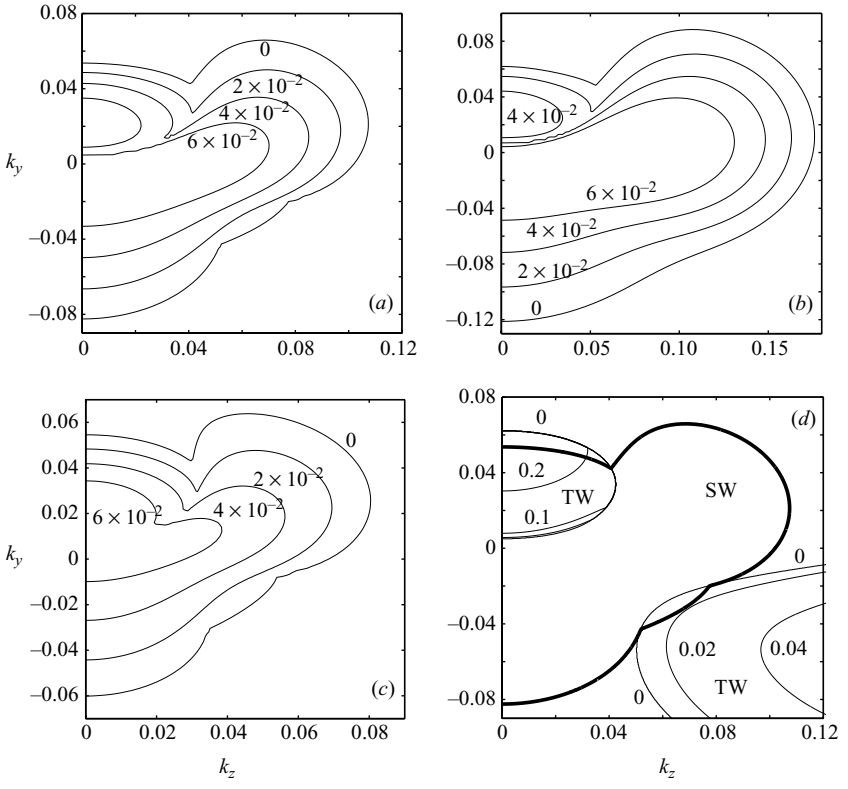


FIGURE 8. Contours of initial growth rates in the (k_z, k_y)-plane for streamwise-dependent perturbations ($k_x = 0.01$) with $e = 0.9$ and $\phi = 0.05$: (*a*) $\beta = -0.9$; (*b*) $\beta = 0.0$; (*c*) $\beta = 1$. (*d*) Contours of frequency ω_i are superimposed on the neutral stability contour (thick line) of (*a*); SW and TW refer to stationary and travelling waves, respectively.

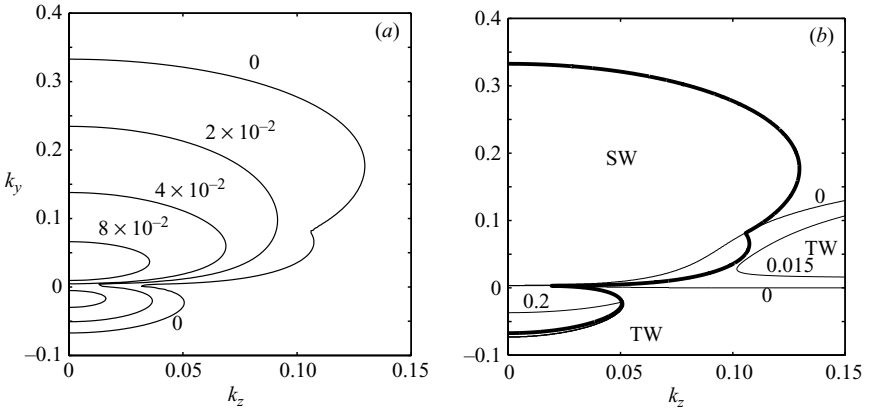


FIGURE 9. (*a*) Same as in figure 8(*a*), but for $\phi = 0.35$. (*b*) Contours of frequency ω_i are superimposed on the neutral stability contour (thick line) of (*a*); SW and TW refer to stationary and travelling waves, respectively.

https://doi.org/10.1017/S002211200600214X Published online by Cambridge University Press

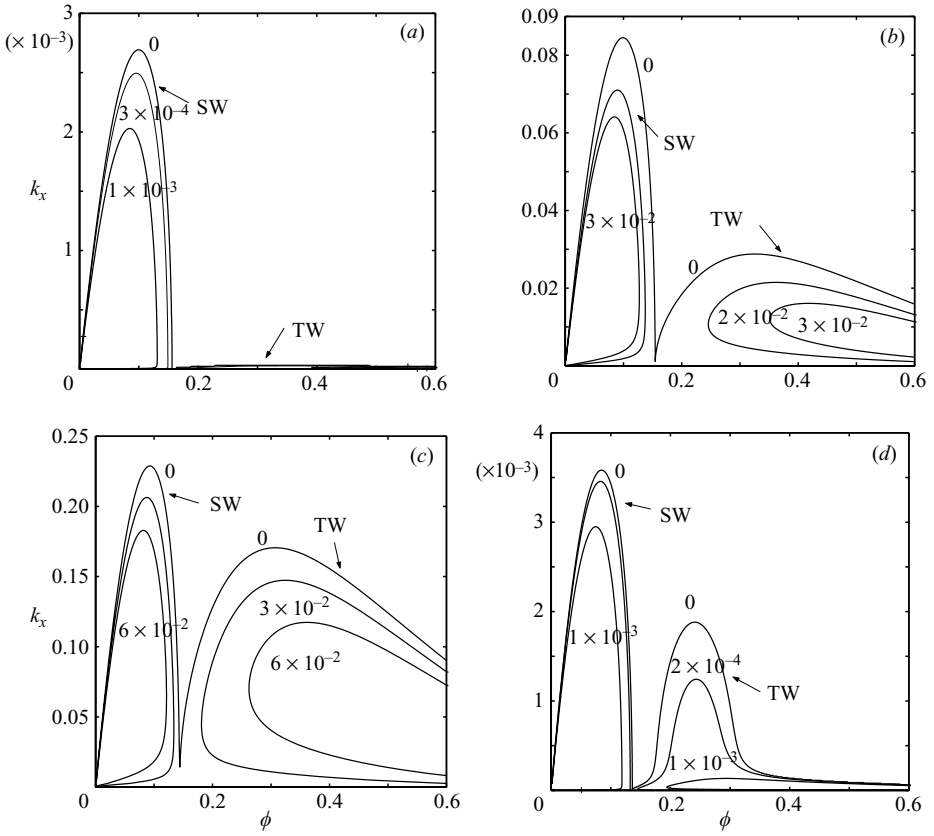


FIGURE 10. Contours of initial growth rates in the (ϕ, k_x)-plane for pure streamwise perturbations ($k_x \neq 0$, but $k_y = 0 = k_z$) with $e = 1.0$: (*a*) $\beta = -0.9999$; (*b*) $\beta = -0.9$; (*c*) $\beta = 0$; (*d*) $\beta = 0.9999$. SW and TW refer to stationary and travelling waves, respectively.

SW. As in the case of dilute flows (figure 8), the dominant instability comes from $k_z = 0$ modes, that holds for higher values of solid fraction too. In contrast to dilute flows, however, the dominant travelling-wave instability for dense flows appears for negative k_y and the dominant stationary instability for positive k_y. Consequently, the orientations of the density patterns for dominant TW and SW modes are reversed for dense flows (compared to those in figure 8 for dilute flows).

All the above results correspond to a low streamwise wavenumber, $k_x = 0.01$. Increasing its value to $k_x = 0.1$ (with other parameters fixed), the growth rate of the least-stable mode as well as the size of the unstable zone increases; however, the travelling waves disappear too, making the stationary waves the least stable modes. With further increase in k_x (to 0.25, say), the flow becomes stable for all k_y and k_z.

Lastly, we show a set of phase diagrams in figure 10 for pure streamwise perturbations ($k_x \neq 0$, with $k_y = 0 = k_z$) for which the wavevectors are aligned along the streamwise direction at $t = 0$. The normal restitution coefficient is set to $e = 1.0$, and the tangential restitution coefficients are (*a*) −0.9999, (*b*) −0.9, (*c*) 0 and (*d*) 0.9999. The flow supports large initial growth rates (and hence unstable, in the above sense) for the whole range of solid fractions for all β except in two limits $\beta \to -1$ and $\beta \to 1$. The instability lobe for dilute flows belongs to stationary waves, but the other one for dense flows to travelling waves. These instabilities become stronger (i.e.

https://doi.org/10.1017/S0022112006002140X Published online by Cambridge University Press

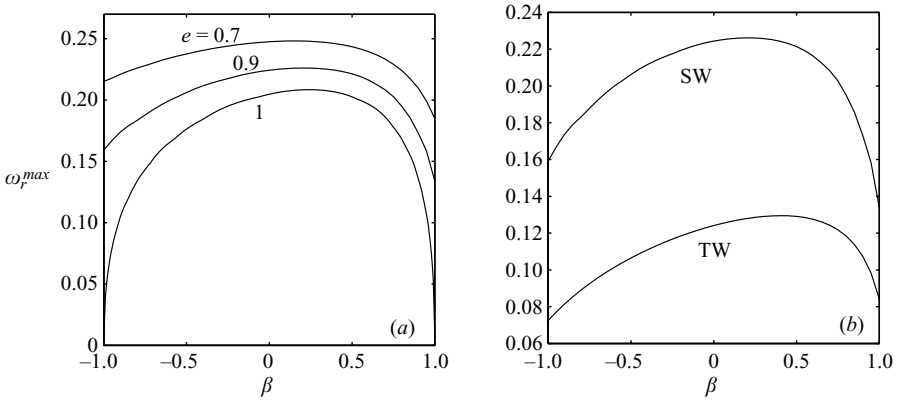


FIGURE 11. (*a*) Variations of the maximum initial growth rate, ω_r^{max} (maximized over the first instability lobe, SW, in figure 10) for pure streamwise perturbations ($k_x \neq 0$, but $k_y = 0 = k_z$) for different e. (*b*) Same as in (*a*), but for both the first (SW) and the second (TW) instability lobes in figure 10 for $e = 0.9$.

the growth rate increases) with increasing dissipation levels ($\sim (1 - e^2)$) for a given value of β, as evidenced in figure 11(*a*) which displays the variations of the maximum growth rate,

$$\omega_r^{max} = \sup_{\phi, k_x} \omega_r^l,$$

with β for three values of e. The dominant instability comes from stationary waves (that correspond to the left instability lobe in figure 10), and that the maximum growth rate for travelling waves remains smaller (by about a factor of two) in comparison with that for stationary waves at any value of β (figure 11*b*). Since for pure streamwise modes (at $t = 0$), the transverse wavenumber is $k_y(t) = -k_x t$, the vertical density bands will degenerate into horizontal bands as $t \to \infty$ (as in the pure transverse instability). Note that the growth rates of these streamwise modes are about two orders of magnitude larger than their pure transverse counterparts in § 5.2 (compare TW instability lobes in figures 10*b* and 10*c* with figures 5*b* and 5*d*, respectively). It is possible that the pure transverse instability (which is stationary) is a consequence of the time-evolution of the pure streamwise 'initial' instabilities (which are travelling waves), via the loss of hyperbolicity of the underlying field equations of perturbation variables – it would be interesting to establish this elusive connection.

Strictly speaking, the above 'exponential' growth of perturbations due to 'initial' growth rates is meaningful if the perturbation-amplitude grows to a sufficiently large value within the time scales of the mean flow such that the nonlinearities in the governing equations can take over to trigger a transition to some new state. (The above comment also holds for the growth of perturbations owing to the inviscid algebraic instability as described in § 5.1.) Since the perturbation time scale is inversely proportional to its growth rate ($\propto 1/\omega_r$), one should closely look at the effect of β on the instability growth rate. It is clear from figure 11(*a*) that the perturbation time scale for $\beta = -1$ differs from that for $\beta > -1$ by a factor of 10 or more in the quasi-elastic limit $e \sim 1$, and this factor decreases to about 2 at $e = 0.9$. Hence, the transient 'exponential' growths are likely to play an important role on the dynamics of rough particles in the quasi-elastic limit.

https://doi.org/10.1017/S002211200600214X Published online by Cambridge University Press

7. Discussion

7.1. *Possible effects of Coulomb friction*

To understand the effects of an small amount of Coulomb friction on the stability characteristics of shear flow, we consider the simplified kinetic theory model of Jenkins & Zhang (2002) who suggested an effective coefficient of normal restitution, in terms of the coefficient of friction μ_f,

$$e_{eff} \approx e - \tfrac{1}{2}\pi\mu_f + 4.5\mu_f^2, \tag{7.1}$$

to account for the additional mechanism of dissipation associated with Coulomb friction. These authors have suggested that we can get dispense with the separate balance equations for the spin fields, and simply solve for the balance equations of smooth particles by incorporating e_{eff} into the dissipation term of the translational energy balance equation. With this modification of e in the reduced set of balance equations, we found that the growth rate of the least stable mode increases with increasing μ_f. However, it is not clear how to recover the non-monotonic dependence of the time and length scales for both spanwise and transverse instabilities on β from such a simplified model. More importantly, this reduced model will miss the algebraic instability-induced momentum transfer mechanism between the translational and the rotational degrees of freedom that we had discussed in § 5.1. Therefore, the full set of balance equations must be used to recover the correct features of the observed instabilities in shear flow.

7.2. *Range of validity of Lun's theory and the higher-order effects*

Here we discuss the validity of Lun's constitutive model (1991) for a micropolar granular fluid with respect to the full range of tangential restitution coefficient $\beta \in (-1, 1)$ as well as the robustness of our reported results. Note that Lun does not use a formal Chapman–Enskog expansion, but uses the moment method (which is akin to the Ritz–Galerkin integral method) to obtain the correction to the equilibrium distribution function: $f = f^0(1 + \psi)$. In the moment method, one chooses a suitable form for the equilibrium distribution function f^0; an appropriate trial function for the correction ψ is then assumed with unknown coefficients that are obtained by satisfying the corresponding higher-order moment equations, and the resulting trial function represents the best possible linear solution. The 'equilibrium' single particle distribution function is taken as:

$$f^0(\boldsymbol{x}_p, \boldsymbol{c}, \boldsymbol{\omega}; t) = \frac{n}{(2\pi T)^{3/2}(2\pi m\theta/\mathscr{I})^{3/2}} \exp\left(-\frac{(\boldsymbol{c}-\boldsymbol{u})^2}{2T}\right) \exp\left(-\frac{\mathscr{I}(\boldsymbol{\omega}-\boldsymbol{\Omega})^2}{2m\theta}\right) \tag{7.2}$$

that allows unequal translational and rotational temperatures at equilibrium, leading to a two-temperature theory. Consequently, Lun's model recovers correct results at both the perfectly rough ($\beta = 1$, Theodosopulu & Dahler 1974) and perfectly smooth ($\beta = -1$, Lun *et al.* 1984) limits.

An important issue is whether we can use Lun's model for the whole range of $\beta \in (-1, 1)$. He obtained a solution for the correction to the equilibrium distribution function, ψ, with the only constraint that the energy dissipation is low (i.e. $e \approx 1$) such that the following term remains small:

$$R_t = \frac{\sigma}{\langle C^2\rangle^{1/2}}\left(\frac{\mathrm{d}u_1}{\mathrm{d}y}\right). \tag{7.3}$$

Indeed this term remains small as long as we restrict ourselves to the quasi-elastic limit $e \approx 1$ for the range of $\beta \in (-1, -0.8)$ and $\beta \in (0.8, 1)$. This term increases by

https://doi.org/10.1017/S002211200600214X Published online by Cambridge University Press

about 5 % (at a volume fraction $\phi = 0.1$) and by 20 % (at a volume fraction $\phi = 0.5$) if we increase β from -1 to 0 at a normal restitution coefficient of $e = 0.8$. Hence, this theory is accurate in the quasi-elastic limit for the whole range of $\beta \in (-1, 1)$. Since our results on instabilities hold at any value of e (irrespective of the value of β), they are valid for any $\beta \in (-1, 1)$.

The above comments on Lun's model are restricted to the Navier–Stokes level of approximation (i.e. first-order in moments as in the moment method, or, equivalently, first-order in the shear rate as in the Chapman–Enskog expansion). To go beyond the quasi-elastic limit, however, we should derive constitutive expressions at the Burnett and super-Burnett levels. For smooth granular particles, such higher-order constitutive models are now available (Sela & Goldhirsch 1998; Chou & Richman 1999; Santos, Garzo & Dufty 2004). One important ingredient of these Burnett-level theories is 'measurable' normal stress differences (Goldhirsch & Sela 1996; Alam & Luding 2003*a*, *b*) that require a separate balance equation for the stress deviator. Moving onto the micropolar description of a granular fluid, we recall that the couple stress appears at the Burnett-level which is known to play an important role near the boundaries (Campbell 1993; Mitarai *et al.* 2002; Goldhirsh *et al.* 2005). We are not aware of any Burnett-order constitutive model for a micropolar granular fluid.

8. Summary and conclusions

We have investigated the linear stability characteristics of an unbounded shear flow of rough granular particles, based on the 'micropolar' constitutive model of Lun (1991). This kinetic-theory-based constitutive model is based on a simple collision model with two material parameters: the normal coefficient of restitution, $0 \leqslant e \leqslant 1$, and the tangential coefficient of restitution, $-1 \leqslant \beta \leqslant 1$. The limit $\beta = -1$ corresponds to perfectly smooth particles, $\beta = 1$ to perfectly rough particles, and $\beta > 0$ represents the case of 'spin-reversal'. For a micropolar continuum, the rotational degrees of freedom give rise to additional balance equations for the angular momentum and the spin granular energy that yield four new hydrodynamic modes in the linear stability analysis which has been carried out using the Kelvin mode decomposition. The base state of the unbounded shear flow is characterized by a linear streamwise velocity profile ($\boldsymbol{u} = (u_x, u_y, u_z) \equiv (u_1, u_2, u_3) = (\dot{\gamma} y, 0, 0)$, where x, y and z are the streamwise, transverse and spanwise directions, respectively, and $\dot{\gamma}$ is the shear rate), with constant values of solid fraction (ϕ), spanwise spin velocity, and translational and spin granular temperatures.

For pure spanwise perturbations ($k_z \neq 0$, but $k_x = 0 = k_y$, where k_i is the wavenumber in the ith direction), we have found that there is an inviscid algebraic instability for the perturbation streamwise velocity $\widehat{u}_1(t)$ that is driven by the perturbation transverse velocity $\widehat{u}_2(0)$, via the mean shear field (u^0_{1y}), such that $|\widehat{u}_1(t)| \to \infty$ as $t \to \infty$ in the inviscid limit (see equations (5.11) and (5.15)). More specifically, $\widehat{u}_2(0)$ extracts momentum from the mean shear and transfers it to $\widehat{u}_1(t)$, leading to this algebraic growth. We have also found that there is algebraic growth of the perturbation transverse spin velocity $\widehat{\Omega}_2(t)$ (see equation (5.13)) which is driven by the coupling of $\widehat{\Omega}_2(t)$ with $\widehat{u}_1(t)$ via the vortex viscosity μ_r. More specifically, the vortex viscosity helps to extract streamwise momentum from $\widehat{u}_1(t)$ and transfers it to the rotational mode $\widehat{\Omega}_2(t)$. This important finding helped us to pinpoint an instability-induced momentum transfer mechanism from the translational degrees of freedom to their rotational counterparts – this is dubbed 'instability-induced rotational-driving' mechanism. It

https://doi.org/10.1017/S0022112006002140X Published online by Cambridge University Press

would be possible to control this mechanism by manipulating with $\widehat{u}_2(0)$, k_z and the base-flow quantities (ϕ^0, T^0, θ^0, μ^0 and μ_r^0), and can also be tested in MD simulations in order to understand the underlying mechanism better.

The above inviscid 'algebraic' instability does not lead to absolute instability for $\widehat{u}_1(t)$ since the viscosity takes over at large times, and $\widehat{u}_1(t)$ (along with $\widehat{u}_2(t)$, $\widehat{\Omega}_1(t)$, $\widehat{\Omega}_2(t)$ and $\widehat{\Omega}_3(t)$) decays in the long-time limit ($t \to \infty$) for pure spanwise perturbations. The other four modes ($\widehat{\phi}$, $\widehat{u}_3$, $\widehat{T}$ and $\widehat{\theta}$) lead to a fourth-order dispersion relation, resulting in an 'exponential' instability for dilute flows (below a critical solid fraction ϕ_c^s) which is stationary in nature. The spin temperature $\widehat{\theta}(t)$ is shown to be a decaying mode, and hence the resulting instability originates from that for perfectly smooth ($\beta = -1$) inelastic ($e \neq 1$) particles. This instability survives even in the limit of perfectly elastic ($e = 1$) but rough ($\beta \neq -1, 1$) particles. With inelastic particles, the effect of the spin fields is to modify the growth rate of this instability (that scales linearly with the spanwise wavenumber in the long-wave limit, i.e. $\omega_r^l \sim k_z$), its length scale (k_z^{-1}) and the corresponding critical solid fraction. In particular, the global maximum growth rate of this instability (maximized over all k_z and ϕ), ω_r^{max}, varies non-monotonically with roughness β, with its value being maximum for intermediate values of β (> 0). The global maximum of the unstable spanwise wavenumber, k_z^{max}, has a similar non-monotonic dependence on β, but the critical solid fraction ϕ_c^s decreases monotonically with increasing β.

For pure transverse perturbations ($k_y \neq 0$, but $k_x = 0 = k_z$), the perturbation fields $\widehat{u}_3(t)$, $\widehat{\Omega}_1(t)$ and $\widehat{\Omega}_2(t)$ are shown to decay with time, and the rest of the stability equations lead to a sixth-order dispersion relation. From a long-wave analysis, we have found that the eigenvalues corresponding to $\widehat{\Omega}_2(t)$ and $\widehat{\theta}(t)$ represent decaying modes, and hence the origin of pure transverse instability is the same as that for smooth but inelastic particles; the growth rate of this stationary instability scales quadratically with the transverse wavenumber (i.e. $\omega_r^l \sim k_y^2$) in the long-wave limit. This instability also survives in the perfectly elastic limit ($e = 1$) of rough particles ($\beta \neq -1, 1$). The global maximum growth rate of this transverse instability, ω_r^{max}, (maximized over all ϕ and k_y) and the global maximum unstable transverse wavenumber, k_y^{max}, vary non-monotonically with roughness β, with their maxima being located at $\beta > 0$; the critical solid fraction ϕ_c^t decreases monotonically with increasing β.

In the perfectly smooth limit ($\beta \to -1$), there is a window of solid fractions, $\phi_c^s < \phi < \phi_c^t$, for which the flow remains stable to all perturbations. However, with the inclusion of spin fields, the size of this window decreases, and at moderate dissipations ($e \sim 0.8$) with $\beta > 0.5$, the flow becomes unstable for all solid fractions. We have found that the two-dimensional perturbations ($k_z = 0$) are most unstable for $\phi > \phi_c^s$ for any value of β, while the three-dimensional perturbations are most unstable for $\phi < \phi_c^s$.

From a long-time analysis of the stability equations for general streamwise-dependent ($k_x \neq 0$) perturbations with $k_y, k_z \neq 0$, we have found that the micropolar granular shear flow remains linearly stable as $t \to \infty$. The effects of the spin fields lead to enhanced decay rates of some hydrodynamics modes owing to the additional damping mechanism of the vortex viscosity. The short-time analysis of these streamwise-dependent perturbations (with $\mathscr{A}(t) = \mathscr{A}_0$ in equation (4.7)), however, revealed that the flow supports 'positive' initial growth rates, owing to both travelling and stationary waves, for all combinations of k_x, k_y and k_z in the long-wave limit, implying that the flow is subject to transient 'exponential' growth of perturbations for $k_x \neq 0$. Such transient growths are important if the instability time scale is such

https://doi.org/10.1017/S002211200600214X Published online by Cambridge University Press

that the perturbation-amplitude can grow to a sufficiently large value within the time scales of the base flow. With the inclusion of spin fields, we have found that the instability time scales are, in general, smaller than that for smooth particles, and this effect becomes increasingly pronounced in the quasi-elastic limit ($e \sim 1$) for which the instability time scale for $\beta > -1$ can differ from that for $\beta = -1$ by an order of magnitude. Hence, the transient 'exponential' growths are likely to play an important role on the dynamics of rough granular particles in the quasi-elastic limit.

The pure spanwise instability corresponds to the 'banding' of particles in the spanwise direction (sometimes called 'vorticity-banding' since the base flow has a non-zero vorticity component along this direction). On the other hand, the pure transverse instability corresponds to 'transverse-banding' of particles (sometimes called 'gradient-banding' since the base flow has gradients along the transverse direction). Both these instabilities belong to a separate class of instabilities, known as 'constitutive' instability (Joseph & Saut 1986; Alam 2006). In particular, both instabilities are short waves in origin, and their short-wave cutoffs are a consequence of the translational and rotational granular conduction terms in the respective energy balance equations. Consequently, both survive in the long-wave limit, and hence the energy balance equations play the role of regularization of the field equations. The inclusion of the spin fields does not change the basic characteristics (e.g. the short-wave origin, the non-monotonic pressure–density curve, the non-monotonic shear-to-pressure ratio and the loss of hyperbolicity; Alam 2006) of these constitutive instabilities.

An important issue is the connection of the present stability results of unbounded shear flow to those of bounded shear flow. As is known for the case of smooth particles, all the reported instabilities would survive in the bounded shear flow as well. However, there are additional instabilities (both stationary and travelling waves) in the bounded shear flow of smooth particles that have no analogue in its unbounded counterpart (Alam & Nott 1998). For a micropolar granular fluid, the bounded shear flow is more complicated owing to the presence of the couple stress which is known to play a prominent role near the boundaries (Campbell 1993; Mitarai *et al.* 2002; Goldhirsch *et al.* 2005). It would be interesting to analyse the stability of the bounded micropolar granular shear flow; work in this direction is in progress.

We acknowledge the computational facilities at the JNCASR as well as the financial support from a grant (PC/EMU/MA/35).

Appendix A. Beyond constant-β collision model: impact angle dependence

The micropolar constitutive model of Lun (1991) is based on a collision model for which the tangential restitution coefficient β is taken to be a constant over the whole range of impact angles (Φ, i.e. the angle between the contact normal and the relative velocity of the contact point), and hence it provides an average description of surface friction. For a more realistic collision model of rough particles with oblique impact, we must take into account Coulomb friction that helps to distinguish between the sliding and the sticking contacts (Maw, Barber & Fawcett 1981; Walton 1992). The complexity of oblique impact has recently been demonstrated by Kuninaka & Hayakawa (2004) who showed that the normal restitution coefficient (e) can exceed unity in the oblique impact of an elastic disk on a soft/hard wall; they also found

https://doi.org/10.1017/S002211200600214X Published online by Cambridge University Press

that e does not exceed unity when the contact angle is controlled by changing the tangential impact velocity with fixed normal velocity. It is clear that a collision model that takes into account all micro-mechanical features of particle collisions still remains a distant reality.

Even though a constitutive model that takes into account the detailed micro-mechanical features of particle collisions is not available, some effort has recently been made to understand the effects of different ingredients of the underlying collision model (see, Huthman & Zippelius 1997; Luding *et al.* 1998; Mitarai *et al.* 2002; Jenkins & Zhang 2002; Hayakawa 2003; Goldhirsch *et al.* 2005; Herbst *et al.* 2005) – this is an active research area. With Walton's collision model which incorporates an impact-angle-dependent tangential restitution coefficient, $\beta(\Phi)$, Herbst *et al.* (2005) shows promising results. They found that while their mean-field theory (based on a pseudo-Liouville operator formalism) with a constant-β approximation provides good agreement with MD simulations (with Walton's collision model) of a homogeneously driven rough granular fluid for $\beta \in (-1, 0.2)$, a variable-β approximation provides excellent agreement for the whole range of $\beta \in (-1, 1)$ for the temperature ratio (θ^0/T^0) as well as for the temporal evolution of translational and rotational temperatures.

The above discussion suggests that a collision model with constant-β provides a reasonable approximation to analyse the dynamics of a rough granular system. For the whole range of β, however, we must consider the impact angle dependence on β. A complete constitutive model based on a 'variable' tangential restitution coefficient with Coulomb friction would be welcome, and may uncover new dynamical features in a driven system like the shear flow.

Appendix B. Coefficient functions in the constitutive model

The non-dimensional coefficient functions, $f_i(\cdot)$, in the expressions of pressure, shear viscosity, bulk viscosity, vortex viscosity are given by (Lun 1991):

$$f_1(\phi; e) := \phi(1 + 4\eta_1 N_1(\phi)), \tag{B 1}$$

$$f_2(\phi, \theta/T; e, \beta, K) := s_{2223}\left[\tfrac{5}{8} + s_{2021} N_1(\phi)\right]\left[\frac{1}{\chi} + s_{24}\phi\right] + s_{25} N_2(\phi), \tag{B 2}$$

$$f_3(\phi; e) := s_{30} N_2(\phi), \tag{B 3}$$

$$f_{2r}(\phi; \beta, K) := s_{20r} N_2(\phi), \tag{B 4}$$

and s_{2021} and s_{2223} are functions of θ/T

$$s_{2021}(\theta/T) = s_{20} + s_{21}\frac{\theta}{T}, \quad s_{2223}(\theta/T) = \frac{1}{s_{22} + s_{23}\,\theta/T}, \tag{B 5}$$

with $N_1(\phi) = \phi\chi$ and $N_2(\phi) = \phi^2\chi$. Here, s_{ij} are functions of e, β and K, given by

$$\left.\begin{aligned} &s_{20} = \eta_1(3\eta_1 - 2) + \tfrac{1}{2}\eta_2(6\eta_1 - 2\eta_2 - 1), \quad s_{21} = -\eta_2^2/K, \\ &s_{22} = 12(2 - \eta_1 - \eta_2)(\eta_1 + \eta_2)/\sqrt{\pi}, \quad s_{23} = -2s_{21}/\sqrt{\pi}, \\ &s_{24} = \tfrac{4}{5}(2\eta_1 + 3\eta_2), \;\; s_{25} = \left(\tfrac{2}{5}/\sqrt{\pi}\right)(4\eta_1 + 3\eta_2), \;\; s_{30} = \left(\tfrac{8}{3}/\sqrt{\pi}\right)\eta_1, \;\; s_{20r} = (2/\sqrt{\pi})\eta_2. \end{aligned}\right\} \tag{B 6}$$

It is clear that $\mu_r \to 0$ as $\beta \to -1$ (i.e. $s_{20r} \to 0$ as $\eta_2 \to 0$) and also as $\phi \to 0$.

https://doi.org/10.1017/S0022112006002140X Published online by Cambridge University Press

The non-dimensional functions for the translational ($\boldsymbol{q}$) and rotational ($\boldsymbol{q}_r$) heat fluxes are given by

$$f_4(\phi,\theta/T;e,\beta,K) := s_{40}\left[\frac{1}{\chi}+s_{41}\phi\right]\frac{\Gamma_2(\phi,\theta/T)}{\Gamma_1(\theta/T)}+s_{42}N_2(\phi), \tag{B 7}$$

$$f_{4h}(\phi,\theta/T;e,\beta,K) := s_{40}\left(\frac{\Gamma_3(\phi)}{\chi\Gamma_1(\theta/T)}\right), \tag{B 8}$$

$$f_{4r}(\phi,\theta/T;e,\beta,K) := s_{40}\left(\frac{1}{\chi}+s_{43}\phi\right)\frac{\Gamma_4(\phi,\theta/T)}{\Gamma_1(\theta/T)}, \tag{B 9}$$

$$f_{4rh}(\phi,\theta/T;e,\beta,K) := s_{40}\left(\frac{1}{\chi}+s_{43}\phi\right)\frac{\Gamma_5(\phi,\theta/T)}{\Gamma_1(\theta/T)}+s_{44}N_2(\phi)\left(\frac{\theta}{T}\right)^{1/2}, \tag{B 10}$$

with the constants s_{ij} being given by

$$s_{40}=\frac{25\sqrt{\pi}}{128},\quad s_{41}=\tfrac{12}{5}\left(\eta_1+\tfrac{2}{3}\eta_2\right),\quad s_{42}=\tfrac{4}{\sqrt{\pi}}(\eta_1+\eta_2),\quad s_{43}=\frac{8\eta_2}{3K},\quad s_{44}=\tfrac{3}{2}s_{43}. \tag{B 11}$$

The functions Γ_i in the expressions of f_{4i} are given by

$$\left.\begin{aligned}
\Gamma_1(\theta/T)&=\tfrac{1}{8}\alpha_1(\theta/T)\alpha_6-\tfrac{25}{24}\alpha_2\alpha_5(\theta/T),\\
\Gamma_2(\phi,\theta/T)&=\tfrac{2}{5}\alpha_3(\phi,\theta/T)\alpha_6+\tfrac{2}{3}\alpha_2\alpha_7(\theta/T)N_1(\phi),\\
\Gamma_3(\phi)&=\tfrac{2}{3}\alpha_2\alpha_8(\phi)+\tfrac{2}{5}\alpha_4\alpha_6N_1(\phi),\\
\Gamma_4(\phi,\theta/T)&=\tfrac{1}{5}\alpha_3(\phi,\theta/T)\alpha_5(\theta/T)+\tfrac{1}{25}\alpha_1(\theta/T)\alpha_7(\theta/T)N_1(\phi),\\
\Gamma_5(\phi,\theta/T)&=\tfrac{1}{25}\alpha_1(\theta/T)\alpha_8(\phi)+\tfrac{1}{5}\alpha_4\alpha_5(\theta/T)N_1(\phi),
\end{aligned}\right\} \tag{B 12}$$

where the expressions for α_i are

$$\left.\begin{aligned}
\alpha_1(\theta/T)&=\alpha_{10}+\alpha_{11}\frac{\theta}{T}, &\alpha_2&=\frac{\eta_2^2}{K},\\
\alpha_3(\phi,\theta/T)&=\frac{5}{2}+\left(\alpha_{30}+\alpha_{31}\frac{\theta}{T}\right)N_1(\phi), &\alpha_4&=\frac{4\eta_2^2}{K}(2\eta_1-1),\\
\alpha_5(\theta/T)&=\alpha_{50}+\alpha_{51}\frac{\theta}{T}, &\alpha_6&=\eta_2\left(1+\frac{7}{3K}-\frac{2\eta_2}{K}-\frac{\eta_2}{K^2}\right)+\eta_1\left(1-\frac{4\eta_2}{3K}\right),\\
\alpha_7(\theta/T)&=\alpha_{70}+\alpha_{71}\frac{\theta}{T}, &\alpha_8(\phi)&=\frac{3}{2}+\alpha_{80}N_1(\phi),
\end{aligned}\right\} \tag{B 13}$$

with constant functions

$$\left.\begin{aligned}
&\alpha_{10}=\eta_1(41-25\eta_1)-8(\eta_1+\eta_2)^2+\eta_2(41-25\eta_2),\quad \alpha_{11}=-\frac{7\eta_2^2}{K},\\
&\alpha_{30}=6\eta_1^2(4\eta_1-3)-4\eta_2(2\eta_1-4\eta_1\eta_2+\eta_2),\quad \alpha_{31}=\frac{8\eta_1\eta_2^2}{K},\\
&\alpha_{50}=\frac{3\eta_2^2}{K},\quad \alpha_{51}=\left(\frac{\eta_2^2}{K^2}-\frac{\eta_2}{K}\right),\\
&\alpha_{70}=\frac{4\eta_2^2}{K}(4\eta_1-1),\quad \alpha_{71}=8\eta_1\left(\frac{\eta_2^2}{K^2}-\frac{\eta_2}{K}\right),\quad \alpha_{80}=\frac{4\eta_2^2}{K^2}(2\eta_1-1).
\end{aligned}\right\} \tag{B 14}$$

https://doi.org/10.1017/S002211200600214X Published online by Cambridge University Press

The non-dimensional functions for the translational ($\mathscr{D}$) and rotational ($\mathscr{D}_r$) dissipations are

$$f_5(\phi, \theta/T; e, \beta, K) := s_{50} s_{5152}(\theta/T) N_2(\phi), \tag{B 15}$$

$$f_{5r}(\phi, \theta/T; \beta, K) := s_{50} s_{5253}(\theta/T) N_2(\phi), \tag{B 16}$$

where s_{5152} and s_{5253} are functions of the temperature ratio

$$s_{5152}\left(\frac{\theta}{T}\right) = s_{51} + s_{52}\frac{\theta}{T}, \quad s_{5253}\left(\frac{\theta}{T}\right) = -s_{52} + s_{53}\frac{\theta}{T}, \tag{B 17}$$

with the constants s_{5j} being given by

$$s_{50} = \frac{48}{\sqrt{\pi}}, \quad s_{51} = \left[\eta_1(1-\eta_1) + \eta_2(1-\eta_2)\right], \quad s_{52} = -\frac{\eta_2^2}{K}, \quad s_{53} = \frac{\eta_2}{K}\left(\frac{\eta_2}{K} - 1\right). \tag{B 18}$$

The non-dimensional parameters η_1 and η_2 are defined via

$$\eta_1 = \frac{(1+e)}{2}, \qquad \eta_2 = \frac{(1+\beta)K}{2(1+K)}. \tag{B 19}$$

In the limit of perfectly smooth spheres ($\beta = -1$), the resulting transport coefficients match those in Lun *et al.* (1984).

Appendix C. Elements of the stability matrix $\mathscr{A}(t)$

The non-zero elements of the time-dependent stability matrix $\mathscr{A}(t)$ are (with $c_p = 1/\phi^0$, $c_k = 8/K\phi^0$, $c_d = 2/3\phi^0$ and $\lambda^0 = \xi^0 - 2\mu^0/3$; $k_y(t) = k_y - k_x t$):

$$\mathscr{A}_{12} = -\mathrm{i}\phi^0 k_x, \quad \mathscr{A}_{13} = -\mathrm{i}\phi^0 k_y(t), \quad \mathscr{A}_{14} = -\mathrm{i}\phi^0 k_z,$$

$$\mathscr{A}_{21} = \mathrm{i}c_p\left[-p_\phi^0 k_x + u_{1y}^0 \mu_\phi k_y(t)\right],$$

$$\mathscr{A}_{22} = -c_p\left[(2\mu^0 + \lambda^0)k_x^2 + (\mu^0 + \mu_r^0)k_y^2(t) + (\mu^0 + \mu_r^0)k_z^2\right],$$

$$\mathscr{A}_{23} = -c_p\left[\phi^0 u_{1y}^0 + (\mu^0 + \lambda^0 - \mu_r^0)k_x k_y(t)\right], \quad \mathscr{A}_{24} = -c_p(\mu^0 + \lambda^0 - \mu_r^0)k_x k_z,$$

$$\mathscr{A}_{26} = -2\mathrm{i}c_p\mu_r^0 k_z, \quad \mathscr{A}_{27} = 2\mathrm{i}c_p\mu_r^0 k_y(t),$$

$$\mathscr{A}_{28} = \mathrm{i}c_p\left[-p_T^0 k_x + u_{1y}^0 \mu_T^0 k_y(t)\right], \quad \mathscr{A}_{29} = \mathrm{i}c_p u_{1y}^0 \mu_\theta^0 k_y(t),$$

$$\mathscr{A}_{31} = \mathrm{i}c_p\left[-p_\phi^0 k_y(t) + u_{1y}^0 \mu_\phi k_x\right], \quad \mathscr{A}_{32} = -c_p(\mu^0 + \lambda^0 - \mu_r^0)k_x k_y(t),$$

$$\mathscr{A}_{33} = -c_p\left[(2\mu^0 + \lambda^0)k_y^2(t) + (\mu^0 + \mu_r^0)k_x^2 + (\mu^0 + \mu_r^0)k_z^2\right],$$

$$\mathscr{A}_{34} = -c_p\left[(\mu^0 + \lambda^0 - \mu_r^0)k_z k_y(t)\right], \quad \mathscr{A}_{35} = 2\mathrm{i}c_p\mu_r^0 k_z, \quad \mathscr{A}_{37} = -2\mathrm{i}c_p\mu_r^0 k_x,$$

$$\mathscr{A}_{38} = \mathrm{i}c_p\left[-p_T^0 k_y(t) + u_{1y}^0 \mu_T^0 k_x\right], \quad \mathscr{A}_{39} = \mathrm{i}c_p u_{1y}^0 \mu_\theta^0 k_x,$$

$$\mathscr{A}_{41} = -\mathrm{i}c_p p_\phi^0 k_z, \quad \mathscr{A}_{42} = -c_p(\mu^0 + \lambda^0 - \mu_r^0)k_x k_z, \quad \mathscr{A}_{43} = -c_p(\mu^0 + \lambda^0 - \mu_r^0)k_y(t)k_z,$$

$$\mathscr{A}_{44} = -c_p\left[(2\mu^0 + \lambda^0)k_z^2 + (\mu^0 + \mu_r^0)k_x^2 + (\mu^0 + \mu_r^0)k_y^2(t)\right],$$

$$\mathscr{A}_{45} = -2\mathrm{i}c_p\mu_r^0 k_y(t), \quad \mathscr{A}_{46} = 2\mathrm{i}c_p\mu_r^0 k_x, \quad \mathscr{A}_{48} = -\mathrm{i}c_p p_T^0 k_z,$$

$$\mathscr{A}_{53} = -\mathrm{i}c_k\mu_r^0 k_z, \quad \mathscr{A}_{54} = \mathrm{i}c_k\mu_r^0 k_y(t), \quad \mathscr{A}_{55} = -2c_k\mu_r^0,$$

https://doi.org/10.1017/S002211200600214X Published online by Cambridge University Press

$$\mathscr{A}_{62} = \mathrm{i}c_k\mu_r^0 k_z, \quad \mathscr{A}_{64} = -\mathrm{i}c_k\mu_r^0 k_x, \quad \mathscr{A}_{66} = -2c_k\mu_r^0,$$

$$\mathscr{A}_{72} = -\mathrm{i}c_k\mu_r^0 k_y(t), \quad \mathscr{A}_{73} = \mathrm{i}c_k\mu_r^0 k_x, \quad \mathscr{A}_{77} = -2c_k\mu_r^0,$$

$$\mathscr{A}_{81} = c_d\big(u_{1y}^{0\,2}\mu_\phi^0 - \mathscr{D}_\phi^0\big), \quad \mathscr{A}_{82} = \mathrm{i}c_d\big[-p^0 k_x + u_{1y}^0\big(2\mu^0 + \mu_r^0\big)k_y(t)\big],$$

$$\mathscr{A}_{83} = \mathrm{i}c_d\big[u_{1y}^0\big(2\mu^0 - \mu_r^0\big)k_x - p^0 k_y(t)\big], \quad \mathscr{A}_{84} = -\mathrm{i}c_d p^0 k_z, \quad \mathscr{A}_{87} = 2c_d u_{1y}^0\mu_r^0,$$

$$\mathscr{A}_{88} = c_d\big[\big(u_{1y}^{0\,2}\mu_T^0 - \mathscr{D}_T^0\big) - \kappa^0\big(k_x^2 + k_y^2(t) + k_z^2\big)\big],$$

$$\mathscr{A}_{89} = c_d\big[\big(u_{1y}^{0\,2}\mu_\theta^0 - \mathscr{D}_\theta^0\big) - \kappa_h^0\big(k_x^2 + k_y^2(t) + k_z^2\big)\big],$$

$$\mathscr{A}_{91} = -c_d\mathscr{D}_{r\phi}^0, \quad \mathscr{A}_{92} = 2\mathrm{i}c_d\mu_r^0\Omega_3^0 k_y(t), \quad \mathscr{A}_{93} = -2\mathrm{i}c_d\mu_r^0\Omega_3^0 k_x, \quad \mathscr{A}_{97} = 4c_d\mu_r^0\Omega_3^0,$$

$$\mathscr{A}_{98} = c_d\big[-\mathscr{D}_{rT}^0 - \kappa_r^0\big(k_x^2 + k_y^2(t) + k_z^2\big)\big],$$

$$\mathscr{A}_{99} = c_d\big[-\mathscr{D}_{r\theta}^0 - \kappa_{rh}^0\big(k_x^2 + k_y^2(t) + k_z^2\big)\big].$$

REFERENCES

Alam, M. 2005 Universal unfolding of pitchfork bifurcations and the shear-band formation in rapid granular Couette flow. In *Trends in Applications of Mathematics to Mechanics* (ed. Y. Wang & K. Hutter), pp. 11–20. Shaker, Aachen.

Alam, M. 2006 Streamwise structures and density patterns in rapid granular Couette flow: a linear stability analysis. *J. Fluid Mech.* **553**, 1.

Alam, M. & Luding, S. 2003*a* Rheology of bidisperse granular mixtures via event-driven simulations. *J. Fluid Mech.* **476**, 69.

Alam, M. & Luding, S. 2003*b* First normal stress difference and crystallization in a dense sheared granular fluid. *Phys. Fluids* **15**, 2298.

Alam, M. & Nott, P. R. 1997 The influence of friction on the stability of unbounded granular Couette flow. *J. Fluid Mech.* **343**, 267.

Alam, M. & Nott, P. R. 1998 Stability of plane Couette flow of a granular material. *J. Fluid Mech.* **377**, 99.

Babić, M. 1993 On the stability of rapid granular flows. *J. Fluid Mech.* **254**, 127.

Babić, M. 1997 Average balance equations for granular materials. *Intl J. Engng Sci.* **35**, 523.

Bender, C. M. & Orszag, S. A. 1999 *Advanced Mathematical Methods for Scientists and Engineers.* Springer.

Cafiero, R., Luding, S. & Herrmann, H. J. 2002 Rotationally driven gas of inelastic rough spheres. *Europhys. Lett.* **60**, 854.

Campbell, C. S. 1993 Boundary interactions for two-dimensional granular flows. Part 1. Flat boundaries, asymmetric stresses and couple stresses. *J. Fluid Mech.* **247**, 111.

Chapman, S. & Cowling, T. G. 1970 *The Mathematical Theory of Non-Uniform Gases.* Cambridge University Press.

Chou, C. S. & Richman, M. W. 1999 Constitutive theory for homogeneous granular shear flows of highly inelastic spheres. *Physica* A **259**, 430.

Condiff, D. W. & Dahler, J. S. 1964 Fluid mechanical aspects of antisymmetric stress. *Phys. Fluids* **6**, 842.

Conway, S. L. & Glasser, B. J. 2004 Density waves and coherent structures in granular Couette flow. *Phys. Fluids* **16**, 509.

Dahler, J. S. & Theodosopulu, M. 1975 Kinetic theory of dense polyatomic fluids. *Adv. Chem. Phys.* **31**, 155.i

Ellingsen, T. & Palm, E. 1975 Stability of linear flows. *Phys. Fluids* **18**, 487.

Goldhirsch, I. 2003 Rapid granular flows. *Annu. Rev. Fluid Mech.* **35**, 267.

Goldhirsch, I. & Sela, N. 1996 Origin of normal stress differences in rapid granular flows. *Phys. Rev.* E **54**, 4458.

https://doi.org/10.1017/S002211200600214X Published online by Cambridge University Press

Goldhirsch, I. & Zanetti, D. 1993 Clustering instability in dissipative gases. *Phys. Rev. Lett.* **70**, 1619.

Goldhirsch, I., Noskowicz, S. H. & Bar-Lev, O. 2005 Nearly smooth granular gases. *Phys. Rev. Lett.* **95**, 068002-1.

Goldshtein, A. & Shapiro, M. 1995 Hydrodynamics of granular materials. *J. Fluid Mech.* **282**, 75.

Hayakawa, H. 2003 Note on a micropolar gas-kinetic theory. In *Traffic and Granular Flows 2001* (ed. M. Fukui, Y. Sugiyama, M. Schreckenberg & D. Wolf), pp. 485–490. Springer.

Herbst, O., Cafiero, R., Zippelius, A., Herrmann, H. J. & Luding, S. 2005 A driven two-dimensional granular gas with Coulomb friction. *Phys. Fluids* **17**, 107102.

Herrmann, H. J., Hovi, J.-P. & Luding, S. 1998 *Physics of Dry Granular Media.* Kluwer.

Hopkins, M. A., Louge, M. Y. & Jenkins, J. T. 1993 Structure of 3D granular shear flows. *Mech. Materials* **16**, 179.

Huthmann, M. & Zippelius, A. 1997 Dynamics of inelastically colliding rough spheres: relaxation of translational and rotational energy. *Phys. Rev.* E **56**, R6275.

Hutter, K. & Rajagopal, K. R. 1994 On flows of granular materials. *Continuum Mech. Thermodyn.* **6**, 81.

Jaeger, H. M., Nagel, S. R. & Behringer, R. 1996 Granular solids, liquids and gases. *Rev. Mod. Phys.* **68**, 1259.

Jenkins, J. T. & Richman, M. W. 1985 Kinetic theory for plane flows of a dense gas of identical, rough, inelastic disks. *Phys. Fluids* **28**, 3485.

Jenkins, J. T. & Zhang, C. 2002 Kinetic theory for identical, frictional, nearly elastic spheres. *Phys. Fluids* **14**, 1228.

Joseph, D. D. & Saut, J. C. 1986 Change of type and loss of evolution in the flow of viscoelastic fluids. *J. Non-Newtonian Fluid Mech.* **20**, 117.

Kadanoff, L. 1999 Built upon sand: theoretical ideas inspired by granular flows. *Rev. Mod. Phys.* **71**, 435.

Kanatani, K. 1979 A micropolar continuum theory for the flow of granular materials. *Intl J. Engng Sci.* **17**, 419.

Kelvin, Lord 1887 Stability of fluid motion. *Phil. Mag.* **24**, 188.

Kuninaka, H. & Hayakawa, H. 2004 Anomalous behaviour of the coefficient of normal restitution in oblique impact. *Phys. Rev. Lett.* **93**, 154301.

Luding, S. & Herrmann, H. J. 1999 Cluster growth in freely cooling granular media. *Chaos* **9**, 673.

Luding, S., Huthmann, M., McNamara, S. & Zippelius, A. 1998 Homogeneous cooling of rough, dissipative particles: theory and simulations. *Phys. Rev.* E **58**, 3416.

Luding, S., Cafiero, R. & Herrmann, H. J. 2003 Driven granular gases. In *Granular Gas Dynamics* (ed. T. Pöschel & N. V. Brilliantov) Lectures Notes in Physics, vol. 624. Springer.

Lun, C. K. K. 1991 Kinetic theory for granular flow of dense, slightly inelastic, slightly rough spheres. *J. Fluid Mech.* **233**, 539.

Lun, C. K. K. & Bent, A. A. 1994 Numerical simulations of inelastic frictional spheres in simple shear flow. *J. Fluid Mech.* **258**, 335.

Lun, C. K. K. & Savage, S. B. 1987 A simple kinetic theory for granular flow of rough, inelastic, spherical particles. *Trans. ASME* E: *J. Appl. Mech.* **54**, 47.

Lun, C. K. K., Savage, S. B, Jeffrey, D. J. & Chepurniy, N. 1984 Kinetic theories for granular flow: inelastic particles in Couette flow and slightly inelastic particles in a general flow field. *J. Fluid Mech.* **140**, 223.

McCoy, B. J., Sandler, S. I. & Dahler, J. S. 1966 Transport properties of polyatomic fluids. IV. The Kinetic theory of a dense gas of perfectly rough spheres. *J. Chem. Phys.* **45**, 3485.

McNamara, S. 1993 Hydrodynamic modes of a uniform granular medium. *Phys. Fluids* **5**, 3056.

McNamara, S. & Luding, S. 1998 Energy non-equipartition in systems of inelastic, rough spheres. *Phys. Rev.* E **58**, 2247.

Maw, N., Barber, J. R. & Fawcett, J. N. 1981 The role of elastic tangential compliance in oblique impact. *Trans. ASME* F: *J. Lubrication Technol.* **103**, 74.

Mello, T. M., Diamond, P. H. & Levine, H. 1991 Hydrodynamic modes of granular shear flow. *Phys. Fluids* A 3, 2067.

Mitarai, N., Hayakawa, H. & Nakanishi, H. 2002 Collisional granular flow as a micropolar fluid. *Phys. Rev. Lett.* **88**, 174301.

https://doi.org/10.1017/S002211200600214X Published online by Cambridge University Press

Montanero, J. M., Garzo, V., Santos, A & Brey, J. J. 1999 Kinetic theory of simple granular shear flows of smooth hard spheres. *J. Fluid Mech.* **389**, 391.

Moon, S. J., Swift, J. B. & Swinney, H. L. 2004 Role of friction in pattern formation in oscillated granular layers. *Phys. Rev.* E **69**, 031301.

van Noije, T. P. C. & Ernst, E. 2000 Cahn–Hilliard theory of unstable granular fluids. *Phys. Rev.* E **61**, 1765.

Santos, A., Garzo, V. & Dufty, J. 2004 Inherent rheology of a granular fluid in uniform shear flow. *Phys. Rev.* E **69**, 061303.

Savage, S. B. 1984 The mechanics of rapid granular flows. *Adv. Appl. Mech.* **24**, 289.

Savage, S. B. 1992 Instability of unbounded uniform granular shear flow. *J. Fluid Mech.* **241**, 109.

Schmid, P. J. & Henningson, D. S. 2001 *Stability and Transition in Shear Flows*. Springer.

Schmid, P. J. & Kytömaa, H. K. 1994 Transient and asymptotic stability of granular shear flow. *J. Fluid Mech.* **264**, 255.

Sela, N. & Goldhirsch, I. 1998 Hydrodynamic equations for rapid shear flows of smooth, inelastic spheres, to Burnett order. *J. Fluid Mech.* **361**, 41.

Tan, M.-L. & Goldhirsch, I. 1997 Intercluster interactions in rapid granular shear flows. *Phys. Fluids* A **9**, 856.

Theodosopulu, M. & Dahler, J. S. 1974 Kinetic theory of dense polyatomic liquids. II. The rough sphere, rigid ellipsoid, and square-well ellipsoid models. *J. Chem. Phys.* **60**, 4048.

Wang, C.-H., Jackson, R. & Sundaresan, S. 1996 Stability of bounded rapid shear flows of a granular material. *J. Fluid Mech.* **308**, 31.

Walton, O. R. 1992 Numerical simulation of inelastic, frictional particle–particle interactions. In *Particulate Two-phase Flow* (Ed. M. C. Roco). Butterworth–Heinemann.

https://doi.org/10.1017/S002211200600214X Published online by Cambridge University Press